A01-16227

AIAA 2001-0322

Soot Research in Combustion Science: Introduction and Review of Current Work

D. L. Urban
NASA Glenn Research Center
Cleveland, OH 44135

and G.M. Faeth
Department of Aerospace Engineering
The University of Michigan
Ann Arbor, MI 48109

39th AIAA Aerospace Sciences Meeting & Exhibit
8-11 January 2001 / Reno, NV

AIAA 2001-0322

SOOT RESEARCH IN COMBUSTION SCIENCE: INTRODUCTION AND REVIEW OF CURRENT WORK

D. L. Urban*
NASA Glenn Research Center, Cleveland, OH 44135

G. M. Faeth†
The University of Michigan, Ann Arbor, MI 48109

Abstract

Current understanding and recent research concerning soot in flames are reviewed, considering soot physical and optical properties, interactions between soot and flow phenomena in flames, the structure of laminar soot-containing premixed and nonpremixed flames, and fundamental mechanisms of soot formation, oxidation, and nucleation. Soot physical and optical properties evolve from poorly understood condensed states near the time of nucleation toward polydisperse fractal aggregates of nearly monodisperse and spherical primary particles mainly consisting of amorphous carbon, as a result of carbonization, surface growth, oxidation and aggregation within flames. Compared to gaseous combustion products, soot exhibits unusual hydrodynamic effects because it has small mass diffusion velocities and it mainly convects by local flow velocities. Promising predictions of the structure of premixed soot-containing flames have been achieved using detailed models of hydrocarbon chemistry and transport but more work along these lines is needed, particularly to establish methods of predicting soot properties and the properties of nonpremixed flame environments. Recent studies of soot formation have demonstrated promising performance for the Hydrogen-Abstraction/Carbon-Addition (HACA) mechanism of soot surface growth, dominated by acetylene and H-radical as reactants, but controversy remains about the role of PAH in soot surface growth, effects of pressure on soot growth have not received much attention, and current understanding of soot nucleation remains very incomplete. Recent studies of early soot oxidation at fuel-rich and nearly-stoichiometric conditions have indicated satisfactory performance of the OH surface oxidation mechanism with a collision efficiency of roughly 10% in both nonpremixed and premixed flames but effects of pressure have received little attention, the transition of the surface oxidation mechanism from OH-dominated to O_2-dominated behavior as soot passes into fuel-lean environments must still be resolved, the properties of soot carbonization are largely unknown, and the final stage of soot oxidation when internal oxidation becomes important is not well understood. Thus, given current limitations about fundamental processes of soot formation and oxidation in flame environments, it appears that continued development of approximate models of soot reaction processes will be needed for simulation of practical combustion processes some time to come in spite of their limitations.

---

*Chief, Microgravity Combustion Science Branch, Microgravity Science Division.

†A.B. Modine Professor, Department of Aerospace Engineering; Fellow, AIAA, corresponding author.

Nomenclature

C_i = mass of carbon oxidized per mole of species i reacted (kg $kgmol^{-1}$)
C_{ij} = aggregate scattering cross section for ij polarization directions (m^2)
d = fuel port diameter (m)
d_p = mean primary soot particle diameter (m)
D_f = mass fractal dimension (-)
E(m) = refractive index function (-), $Im((m^2-1)/(m^2+2))$
F(m) = refractive index function (-), $|(m^2-1)/(m^2+2)|^2$
f_s = soot volume fraction (-)
Fr = burner exit Froude number (-), $u_o^2/(gd)$
g = acceleration of gravity (ms^{-2})
i = $(-1)^{1/2}$
[i] = molar concentration of species i (kgmol m^{-3})
k = Boltzman constant (J $molecule^{-1}$ K^{-1})
k_f = mass fractal prefactor (-)
k_n = soot nucleation rate constant ($m^3kgmol^{-1}s^{-1}$)
m = complex refractive index of soot (-), $n+i\kappa$
M_i = molecular weight of species i (kg $kgmol^{-1}$)
n = real part of refractive index of soot (-)
n_p = number of primary particles per unit volume (m^{-3})
N = number of primary particles per aggregate (-)
R_i = terms in the HACA soot surface growth rate formulas (kg $m^{-2}s^{-1}$)
Re = burner exit Reynolds number (-), u_od/ν_o
R_g = radius of gyration of an aggregate (m)
S = soot surface area per unit volume (m^{-2})
t = time (s)
T = temperature (K)
u = streamwise velocity (ms^{-1})
v_i = molecular velocity of species i (ms^{-1})
w_g = soot surface growth rate (kg $m^{-2}s^{-1}$)
w_{ox} = soot surface oxidation rate (kg $m^{-2}s^{-1}$)
w_n = soot nucleation rate (mole $m^{-3}s^{-1}$)
x_p = primary particle optical size parameter (-), $\pi d_p/\lambda$
z = streamwise distance (m)
α_i = empirical (steric) factors in HACA soot surface growth rate formulas
η_i = collision efficiency of species i
θ = angle of scattering from the forward direction (deg)
κ = imaginary part of refractive index of soot (-)
ν = kinematic viscosity (m^2s^{-1})
λ = wavelength of radiation (m)
ρ = gas density (kg m^{-3})
ρ_s = soot density (kg m^{-3})
ϕ = fuel-equivalence ratio (-)

Subscripts

CH = HACA soot growth mechanism of Colket and Hall[111]
FW = HACA soot growth mechanism of Frenklach and coworkers[106-110]
h = horizontal polarization
ij = incident (i) and scattered (j) polarization direction
o = burner exit condition
v = vertical polarization

Superscripts

(-) = mean value

Introduction

The presence of soot is a ubiquitous feature of nonpremixed flames fueled with hydrocarbons, affecting their structure, their transport and their reaction mechanisms. As a result, soot properties and processes affect capabilities for computational combustion due to the complexities of soot chemistry, affect public health due to pollution problems resulting from emissions of particulate soot, affect fire safety due to increased fire spread and growth rates caused by soot radiation and emissions of toxic substances associated with soot emissions, and combustor durability due

to undesirable heat loads caused by continuum radiation from soot. Motivated by these observations, there have been numerous studies of soot phenomena in flame environments. It is the objective of this article to review current understanding concerning soot in flames resulting from this work, and to suggest areas where additional research is needed.

Various soot properties and processes in flame environments have been reviewed in the past. In particular, the classical early review article about soot reaction properties due to Palmer and Cullis,[1] has been periodically updated by others, including Wagner,[2] Haynes and Wagner,[3] Donnet,[4] Glassman,[6] Howard[7] and Kennedy.[8] In addition, Donnet,[4] Jullien and Botet[9] and Köylü and Faeth[10,11] have reviewed current understanding of soot structure and optical properties whereas Alden[12] provides an overview of optical techniques for measuring soot properties in flames. The goal of the present article is to extend these discussions up to the present, in order to provide both an introduction to soot process in flames and to suggest directions for future research.

The article begins with consideration of the physical and optical properties of soot and the interesting interactions between soot and fluid flow processes that result because soot has small mass diffusivities and mainly is transported by convection. Soot reactive properties are then introduced by considering the environment of soot in flames in both premixed and nonpremixed flames. Then recent progress toward gaining an understanding of soot formation and oxidation in flame environments is discussed by describing recent experimental evaluations of detailed models of soot growth, oxidation and nucleation. The various sections contain their own summaries and conclusions so that they can be read independently.

Soot Physical Properties

The physical properties of soot particles will be considered first in order to provide background needed to understand their optical, transport and reactive properties. Soot particles have a reasonably generic structure in both nonpremixed and premixed flames based on Transmission Electron Microscope (TEM) photographs that have appeared in the literature, see Dalzell et al.,[13] Dobbins and Megaridis,[14] Erickson et al.,[15] Faeth and Köylü[11], Köylü and Faeth,[10,16] Medalia and Heckman,[17] Nelson,[18] Samson et al.,[19] and Wersborg et al.[20] for examples. A typical TEM photograph of a soot particle appears in Fig. 1. These conditions involve soot emitted from a nonbuoyant round ethylene-fueled laminar jet diffusion flame burning in still air at 100 kPa, obtained during an experiment carried out at microgravity conditions on board the Space Shuttle Columbia.[21,22] The soot particle in the photo is large due to its long residence time in the nonbuoyant laminar diffusion flame but is otherwise representative of soot found in flame environments.

Detailed measurements of soot particles indicate that they consist of nearly spherical primary soot particles having relatively uniform diameters at a given flame condition that aggregate to form open-structured particles (aggregates). In particular, measurements of primary particle diameters of soot aggregates emitted from large buoyant turbulent diffusion flames in the long residence time regime, where soot properties in the fuel-lean (overfire) region are generally independent of position and residence time, yielded probability density functions that generally satisfied Gaussian distributions with mean primary particle diameters smaller than 60 nm and standard deviations smaller than 25% and with mean primary particle diameters ordered following the fuel's propensity to emit soot.[16] This behavior generally has been observed for soot aggregates at a variety of flame conditions.[9-24] The primary particles tend to be somewhat merged, rather than just touching at points, due to soot growth subsequent to the joining of adjacent primary particles. Models of soot aggregates as monodisperse spherical primary particles that just touch one another, however, are a reasonable approximation of TEM observations, e.g., Fig. 1, and this approximation generally has been adopted for studies of soot optical properties.[9-26]

Other important physical properties of soot aggregates include their density, porosity and composition. Not surprisingly, these properties generally are similar to the properties of carbon blacks, however, there

are two major exceptions: soot during the last stages of oxidation has significant porosity, even extending to the presence of hollow cenospheres,[27] and soot from some internal engine combustion processes (such as diesel engines at heavily sooting conditions) contain surprisingly large levels of volatile matter.[28] Otherwise, soot densities are typical of carbon blacks, with values in the range 1820-2050 kg/m^3, see Dobbins et al.,[29] Wu et al.[30] and references cited therein. Soot aggregates also appear to be relatively nonporous with quantitative (BET) measurements of surface area compatible with shapes observed on TEM photographs except as noted earlier. Soot also mainly consists of carbon except for the small primary particles of recently nucleated soot. For example, soot emitted from long residence time buoyant turbulent diffusion flames (involving the combustion of toluene, benzene, acetylene, propylene and propane burning in air) had the following elemental mole ratio ranges: C/H of 8.3-18.3, C/O of 58-109 and C/N of 292-976.[11] However, the presence of volatiles, as well as annealing (carbonization) processes at high temperatures, affect concentrations of noncarbon substances in soot, and possibly optical properties such as soot refractive indices as well.[31-36]

The uniformity of primary soot particles also is an issue because this can affect soot oxidation and optical properties and is an indication of fundamental changes of the soot formation mechanism as a soot aggregate moves through a flame environment. Thus, a number of workers have undertaken soot primary particle microstructure studies using High Resolution Transmission Electron Microscopy (HRTEM), see Lahaye and Prado,[28] Dobbins et al.,[29] Ishiguro et al.[37] and references cited therein. These studies generally show that primary soot particles contain a variety of internal structures depending on the point in the soot particle life history and within the flame where particular regions of the primary particle were formed. The most common variation of internal structure that is seen, however, is the somewhat different structure near the core (at conditions near nucleation of the particle) and near the surface of the primary particles. This behavior is illustrated by the sketch of soot emitted from a diesel engine due to Ishiguro et al.[37] that is illustrated in Fig. 2. It is clear that the structure near the center of the primary soot particles, resulting from coalescence of large PAH molecules to form a nucleation site, is very different from the more layered and regular structure resulting from soot growth near the surface of the primary soot particle. Thus, whereas models of soot optical and reaction properties generally adopt approximations of uniform primary soot properties, and ignore potential variations of refractive indices and surface structure with fuel type and flame conditions as a result, these approximations clearly merit additional scrutiny.

As noted earlier, mean primary soot particle densities vary with flame conditions and fuel type but diameters less than 60 nm generally are observed in flame environments. This implies that values of the primary particle optical size parameter, $x_p < 0.4$ for $\lambda > 500$ nm; as a result, it is reasonable to assume that individual primary particles behave similar to Rayleigh scattering particles, e.g., total scattering and absorption cross sections are within 1% and 5%, respectively, of estimates based on the Rayleigh scattering approximation for individual primary particles using currently accepted values of the refractive indices of soot.[10,26,38] In spite of these properties, however, it has long been recognized that soot aggregates are not effectively modeled by the Rayleigh scattering approximation.[15,20] This difficulty comes about because soot aggregates contain numerous primary particles and have dimensions that are comparable to wavelengths associated with ultraviolet, visible and infrared wavelength ranges of interest for soot optical diagnostics and estimates of the continuum radiation properties of soot, e.g., the largest dimension of the soot aggregate illustrated in Fig. 1 is 1200 nm. In order to properly consider the behavior of soot optical properties, the structure properties of soot aggregates must be known; therefore, these properties will be considered next.

Soot aggregates are small at nucleation conditions but they aggregate rapidly in flame environments with the average number of primary particles per aggregate, N, in the range 200-600 for soot emitted from buoyant turbulent diffusion flames in the long

residence time regime.[23,24] Unlike primary particle diameters, however, aggregate size distributions are very broad, with standard deviations comparable to $\bar{N}$ and large values of the second moment of the distribution, e.g., values of $\bar{N^2}/(\bar{N^2})$ of 2.0-3.3 have been observed for soot emitted from buoyant turbulent diffusion flames in the long residence time regime.[23] Aggregate size distributions are represented reasonably well by a log normal distribution function, however, which simplifies determination of averages of optical properties over the aggregate size range.[14,15,28] Based on the properties of log normal distribution function, 95% of the aggregates emitted from large buoyant turbulent diffusion flames in the long residence time regime contain 30-1800 primary particles. This means that the optical properties of soot aggregates are complex for wavelengths of interest for soot processes ranging from Rayleigh scattering for small aggregates, where each primary particle essentially scatters light independently, to significant interactions between scattering from individual primary particles for large aggregates. Fortunately, the treatment of the optical properties of such soot populations is simplified considerably by the fact that soot aggregates are classical mass fractal-like objects as discussed next.

Numerous evaluations have shown that flame-generated soot aggregates exhibit mass fractal-like behavior with a Hausdorf or mass fractal dimension, $D_f < 2$, even when the number of primary particles in an aggregate is small, see Refs. 9, 10, 11, 16, 19, 22, 23, 30, 38 and 39. Stochastic simulations of the aggregation process due to Mountain and Mulholland[40] suggest that this is a natural consequence of cluster/cluster aggregation that progressively builds up aggregate size and yields size scaling relationships representative of fractal behavior. Furthermore, the value of the fractal dimension has important implications for soot optical properties because the scattering per primary particle continues to grow as the size of the aggregate increases for $D_f > 2$ but reaches a constant saturated value for $D_f < 2$, see Nelson,[18] Berry and Percival,[41] and Dobbins and Megaridis.[42]

The mass fractal approximation implies the following relationship between the primary particle diameter, the number of primary particles, and the radius of gyration of an aggregate:[9]

$$N = k_f(R_g/d_p) \qquad (1)$$

where k_f is the fractal prefactor and the aggregates are assumed to consist of monodisperse nonoverlapping primary particles. Evaluations of the fractal properties of soot aggregates, D_f and k_f, indicate that they are relatively durable properties of soot in flame environments, unlike other aggregate structure properties. Evaluations of fractal dimensions based on scattering measurements involving relatively large soot aggregates emitted from buoyant turbulent diffusion flames in the long residence time regime yielded values relatively independent of fuel type and properly independent of wavelength, with mean values of 1.81 and a standard deviation of 0.02.[26] Recent studies of soot within laminar diffusion flames, where soot aggregates are still developing and are relatively small, yielded similar values of fractal dimensions, in the range 1.7-1.8, also relatively independent of fuel type.[10,39]

Fractal prefractors are much more difficult to measure than fractal dimensions and have received much less attention. Early determination of k_f by measurements due to Sorensen et al.[43] and numerical simulations due to Mountain and Mulholland[40] yielded relatively low values, e.g., the simulations of Mountain and Mulholland[40] yielded k_f of roughly 5.5 for N greater than 10. More recent work yielded values of k_f roughly twice as large: the numerical simulations of k_f of Farias et al.[25] yields k_f of 8.0; scattering measurements of Köylü and Faeth[23] yielded a mean value of k_f of 8.1 with a standard deviation of 0.8, relatively independent of fuel type for soot emitted from buoyant turbulent diffusion flames in the long residence time regime; thermophoretic sampling measurements analyzed by Puri et al.[44] yielded $k_f = 8.6$ and 9.4 for soot aggregates in ethylene- and acetylene-fueled laminar jet diffusion flames burning in air; and thermophoretic sampling measurements of Köylü and Faeth[22] yielded a mean value of k_f of 8.5 with a standard deviation of 1.0 relatively independent of fuel type for soot emitted from large buoyant turbulent diffusion flames in the long residence time regime. The last determination is felt to be the most reliable because it was found from actual

enumeration of soot aggregates using stereoscopic measurements to provide three-dimensional information about aggregate structure and is independent of the relatively large uncertainties of k_f from scattering measurements due to the corresponding relatively large uncertainties of soot refractive indices. Nevertheless, k_f is a critical structure parameter needed to specify the fractal properties of soot aggregates and to estimate soot scattering properties that clearly merits additional study in the future.

Soot Optical Properties

Early attempts to model soot optical properties were based on classical theories using either the Rayleigh scattering approximation at the small particle limit where individual primary soot particles are assumed to scatter independent of the presence of other primary particles in soot aggregates, or the Mie scattering approximation for an equivalent spherical particle (a spherical particle having the same total volume as the aggregate) after postulating some spherical particle size distribution to account for the polydisperse size distribution of soot aggregates. Even early studies of soot in flames demonstrated rather conclusively, however, that neither of these approaches was satisfactory, see Dalzell et al.,[13] Erickson et al.,[15] Wersborg et al.[20] and Magnussen.[45] In particular, many soot aggregates were too large for reasonable application of the Rayleigh scattering approximation, and too open-structured for proper representation as equivalent compact spheres using the Mie scattering approximation. Furthermore, direct measurements and numerical simulations confirmed concerns about approximate modeling of soot scattering properties: strong forward scattering was observed that is not representative of Rayleigh scattering behavior where scattering intensities are independent of direction; whereas, direct use of the Mie scattering approximation for equivalent spheres did not provide an adequate fit of scattering data, see Refs. 10, 13, 15 and 20. Later study of the scattering properties of fractal aggregates helped explain the failure of the Mie scattering approximation for equivalent spheres, e.g., $D_f < 2$ for soot aggregates which implies that scattering per primary particle reaches a constant saturated value as aggregate size increases, rather than continuing to grow with increasing size which would be the case for both $D_f > 2$ and for the Mie scattering approximation for equivalent spheres.

In view of the difficulties encountered when using the Rayleigh and Mie scattering approximations for soot optical properties, recent work has focused on the Rayleigh-Debye-Gans (RDG) scattering approximation. The RDG scattering approximation implies that effects of multiple- and self-scattering are ignored so that the electromagnetic field within each primary particle is the same as the incident field, and differences between the phase shift of light scattered from various points within a particular primary particle are ignored. This requires that both $|m-1| << 1$ and $2x_p|m-1| << 1$,[46-48] where m is the complex refractive index of soot, $n + i\kappa$, which is questionable due to the relatively large refractive indices of soot at both visible and infrared wavelengths.[26,30] In addition, early computational studies suggested significant effects of multiple scattering for typical soot aggregates, see Nelson,[18] Berry and Percival,[41] Chen et al.[49] and Ku and Shen.[50] Thus, the RDG scattering approximation was evaluated using both scattering measurements and numerical simulations as discussed in the following.

Major assumptions of the RDG scattering theories for the optical properties of soot aggregates are as follows: spherical primary particles having a constant diameter, primary particles do not overlap but just touch one another, the refractive indices and densities of primary particles are independent of position within the particle (they are assumed to be uniform), aggregates satisfy log normal size distributions for the number of primary particles per aggregate, the aggregates are mass fractal-like objects that satisfy Eq. 1 with constant values of D_f and k_f, and finally, it should be noted that under the RDG approximation, individual primary particles satisfy the Rayleigh scattering approximation. The resulting combined theory involving both the optical and structure properties of soot aggregates is commonly called the Rayleigh-Debye-Gans-Polydisperse-Fractal-Aggregate (RDG-PFA) scattering theory.[23,24] RDG-PFA

scattering theory is based on methods described by Freltoft et al.,[37] Lin et al.,[52] Martin and Hurd,[53] Jullien and Botet,[9] and Dobbins and Megaridis,[42] as extended by Köylü and Faeth[23] for polydisperse aggregate populations. The formulation is lengthy, however, and will not be repeated here; original sources should be consulted for details.

Evaluation of RDG-PFA predictions was undertaken considering measurements of scattering from soot emitted from buoyant turbulent diffusion flames in the long residence time regime,[23,26,30,38] considering measurements of soot in the fuel-rich region of laminar diffusion flames,[24] and considering numerical simulation of scattering in the small-angle (Guinier) scattering regime that is difficult to access with experiments.[25] Typical examples of experimental evaluations of RDG-PFA theory are illustrated in Figs. 3 and 4. These results include measured and predicted differential scattering cross sections as a function of the scattering angle measured from the forward scattering direction (scattering patterns), considering vv, hh, hv and vh polarization of the incident and scattered light. Figure 3 illustrates the scattering pattern for relatively small soot aggregates at fuel-rich conditions within a laminar diffusion flame; whereas, Fig. 4 illustrates the scattering pattern for relatively large soot aggregates emitted from a buoyant turbulent diffusion flame in the long residence time regime. The predictions are seen to be in excellent agreement with the measurements in both cases (the discrepancies between measurements and predictions of the hv and vh scattering cross sections at small angles are solely due to experimental difficulties and are not due to a deficiency of RDG-PFA theory, as discussed in Ref. 23). Comparing the results of Figs. 3 and 4 also illustrates the effect of aggregate size on scattering properties with the very strong forward vv scattering observed for large aggregates evolving toward uniform vv scattering, that is more typical of Rayleigh scattering,[47] as the aggregates become smaller. Similar performance of RDG-PFA theory has been observed for large aggregates (aggregate distributions having aggregates containing up to 500-2000 primary particles) for wavelengths of 250-800 nm and primary particle size parameters, $x_p < 0.46$. This suggests that RDG-PFA theory provides a relatively robust approach for treating the optical properties of soot for conditions of practical interest. Current limitations about soot optical property predictions, as well as reasons for the good performance of RDG-PFA theory for soot properties at wavelengths of interest for soot, follow from the refractive index properties of soot which will be considered next.

Given reasonably good performance of RDG-PFA theory for treating the optical properties of populations of soot aggregates at wavelengths of interest for practical applications, it was concluded that estimates of soot optical properties were mainly limited by excessive uncertainties about soot refractive index properties, see Refs. 26, 30, 38, 54 and references cited therein. This prompted several *in situ* studies of soot optical properties, where data was reduced to find refractive index properties based on RDG-PFA theory, considering soot emitted from buoyant turbulent diffusion flames in the long residence time regime. Naturally, the real and imaginary parts, n and κ, of the complex refractive index function, m, of any substance are of great fundamental importance in their own right, however, the following discussion will be limited to the refractive index functions for absorption and scattering, E(m) and F(m), because these functions directly affect the optical properties of soot under the RDG scattering approximation,

Recent measurements of E(m) and F(m), reported as F(m)/E(m) and E(m), are illustrated in Figs. 5 and 6, for wavelengths of 250-10000 nm. Values of F(m)/E(m) include the *ex situ* reflectometry measurements of Dalzell and Sarofim,[51] Stagg and Charalampopoulos[52] and Felske et al.[53] and the *in situ* absorption and scattering measurements of Krishnan et al.[26] and Wu et al.[30] The results of Dalzell and Sarofim[51] are averages of measurements for acetylene- and propane-fueled flames burning in air, whereas the other results are averages of measurements for acetylene-, ethylene-, propane-, propylene-, benzene-, toluene-, cyclohexane- and n-heptane-fueled flames burning in air; in general, effects of fuel type on values of F(m)/E(m) and E(m) were small. Except for the *ex situ* measurements of Dalzell and

Sarofim,[51] all the measurements of F(m)/E(m) illustrated in Fig. 5 are in reasonably good agreement. Similar results for E(m) are illustrated in Fig. 6, with the *ex situ* measurements of Dalzell and Sarofim,[51] and Felske et al.[53] illustrating the greatest departure from the average of the rest of the measurements. The general tendency for the scattering properties of these soot populations to remain relatively large with increasing wavelength in spite of the general behavior of RDG scattering objects to have progressively reduced scattering with increasing wavelength, however, requires compensating increases of E(m) and F(m) with increasing wavelength which raises questions about the measured results of Refs. 51 and 53. Nevertheless, resolving discrepancies between the *in situ* and some of the *ex situ* measurements of E(m) and F(m) seen in Figs. 5 and 6 merits priority because these differences can have a large impact on the interpretation of optical diagnostics of soot properties and estimates of continuum radiation from soot.

The results concerning E(m) and F(m) as a function of wavelength also highlight two other important properties concerning absorption and scattering of soot in the visible and infrared wavelength ranges. First of all, the RDG scattering approximation remains effective over this range because effects of scattering are small at long wavelengths which implies good performance for the RDG scattering approximation as expected; on the other hand, deterioration of the RDG scattering approximation which would be expected at small wavelengths for constant refractive indices,[46-48] does not occur because soot refractive indices fortuitously become small at these conditions rather than becoming large due to approach to a resonance condition in the near ultraviolet which is observed for graphite which also is a carbonaceous material.[52,53] Finally, the rather large increase of F(m)/E(m) tends to maintain significant levels of scattering from soot within the near infrared which was not expected by early workers;[53] therefore, past assumptions about the relative unimportance of scattering from soot for optical diagnostics and continuum radiation from soot in the infrared need to be reconsidered based on the results of Figs. 5 and 6.

Soot/Flow Interactions

The current relatively poor understanding of turbulent flows in general and turbulent reactive flows in particular has prompted most fundamental studies of soot phenomena in flames to be limited to laminar flames. In particular, the regions involving significant soot reaction processes in turbulent flames tend to be thin, causing problems of limited spatial resolution, and unsteady, causing problems of limited temporal resolution, for both measurements and numerical simulations. Thus, the use of steady laminar flames for studies of soot processes in flames, which mitigates problems of both limited spatial and temporal resolution, is very attractive and most fundamental studies of soot processes in flame environments have been carried out using laminar conditions. Certainly it can be argued that a full understanding of soot phenomena in turbulent flames is unlikely to precede comparable understanding of soot phenomena in laminar flames. Thus, the following considerations of the reaction properties of soot in flames will be limited to consideration of laminar flames.

When using laminar flames as a test environment to study soot processes, it is important to recognize soot/flow interactions that may be different for laminar flames than practical flames that generally are turbulent. In particular, flow velocities are small in typical laminar flames so that effects of buoyancy are much more important for laminar flame conditions than they are for practical turbulent flames. This introduces a subtle problem when buoyant laminar diffusion flames (noting that diffusion flames are of greatest interest for studies of soot processes) are used as tractable flame models for more practical turbulent diffusion flames when processes concerning condensable materials such as soot are being considered. As noted earlier, effects of buoyancy are small in the soot reaction regions of practical turbulent diffusion flames; therefore, buoyant laminar diffusion flames can only provide a proper model flame system of practical turbulent diffusion flames to the extent that effects of buoyancy do not directly affect fundamental soot processes. Unfortunately,

soot particles are too large to diffuse like gas molecules and primarily are convected at local flow velocities; this can result in different behavior in buoyant and nonbuoyant laminar diffusion flames and thus in buoyant laminar diffusion flames and in turbulent diffusion flames. The difficulty can be seen by considering Fig. 7 where some features of buoyant and nonbuoyant laminar jet diffusion flames are plotted as a function of streamwise and radial positions. The results for the buoyant flame are based on measurements,[56-65] whereas the results for the nonbuoyant flames are based on predictions.[66,67] Soot formation reactions in diffusion flames occur where fuel-equivalence ratios are roughly in the range ϕ = 1-2, which is marked on the plots.[5,59,60,61,68,69] The dividing streamline, which is the boundary of the cross section of the flow that has the same streamwise mass flow rate as the burner port (and roughly coincides with the condition of small cross stream velocities), and some typical soot pathlines are also marked on the plots.

In order to interpret Fig. 7, it should be recalled that soot convects with the flow velocity (i.e., diffusion of soot due to Brownian motion and thermophoresis is small compared to convective transport) and moves toward the dividing streamline in the radial direction (because velocities inside and outside the dividing streamline are positive and negative, respectively). The flow accelerates in buoyant flames, therefore, the dividing streamline moves toward the flame axis with increasing streamwise distance and generally lies within the soot formation region. In contrast, the flow decelerates in nonbuoyant flames; therefore, the dividing streamline moves away from the axis with increasing streamwise distance and generally lies outside the soot formation region. The different relative positions of the soot formation regions and the dividing streamlines, and the different degrees of flow acceleration, imply very different scalar-property/time histories for the soot found in buoyant and nonbuoyant flames. For buoyant flames, most of the soot nucleates near the outer boundary of the soot formation region (near the flame sheet at ϕ = 1) and then moves radially inward to cooler and less reactive conditions at larger fuel-equivalence ratios before finally crossing the flame sheet near its tip within an annular soot layer in the vicinity of the dividing streamline. (This type of soot path is denoted as *soot-formation* path by Kang et al.[70]) In contrast, for nonbuoyant flames, most of the soot initially nucleates at relatively large fuel-equivalence ratios near the inner boundary of the soot formation region (near ϕ=2) and thus is drawn directly toward and across the flame sheet, so that it only experiences a monatomic reduction of the fuel-equivalence ratio (This type of soot path is denoted as *soot-formation-oxidation* path by Kang et al.[70]). In addition, velocities along these soot paths progressively increase (decrease) with increasing distance along the path for buoyant (nonbuoyant) laminar jet diffusion flames, respectively, which implies that ratios of soot-formation/soot-oxidation times generally are larger for buoyant than for nonbuoyant flames.

In view of these considerations, soot processes within buoyant and nonbuoyant laminar diffusion flames clearly are very different, with results for nonbuoyant laminar diffusion flames representing the soot processes that are of greatest interest for practical turbulent diffusion flames (which generally only exhibit small effects of buoyancy due to large flow velocities). These observations have motivated the use of microgravity conditions for general experimental studies of flow/soot interactions and the behavior of soot in nonbuoyant flames as a model for soot processes in turbulent flames, see Refs. 21, 33, 58, and 71-74. Detailed experimental studies of the structure and soot reaction processes of laminar diffusion flames require extensive instrumentation and test times, however, which generally are not available for experiments at microgravity conditions. This has led to studies of buoyant laminar diffusion flames using ground-based facilities which at least represent the major features of nonbuoyant flames. One approach toward this objective is to carry out experiments at low pressures, where effects of buoyancy are substantially reduced.[75] Another approach, when seeking test results at normal pressures, is to confine attention to conditions where soot follows *soot-formation-oxidation* paths so that the reaction properties of soot at least are qualitatively similar to soot behavior in nonbuoyant laminar and turbulent diffusion

flames (although effects of different soot-formation/soot-oxidation residence times due to the decelerating and accelerating flow velocities of nonbuoyant and buoyant flames still cannot be simulated). The partial simulation can be carried out by recognizing that soot paths that are nearer to the axis of buoyant laminar diffusion flames than the dividing streamlines still properly follow *soot-formation-oxidation* paths. Finally, as a practical matter, such conditions are most conveniently provided by limiting measurements to the axes of buoyant laminar diffusion flames which is the approach that has been used in all studies of structure and soot properties of laminar diffusion flames to be discussed in the following.

Structure of Premixed Soot-Containing Flames

Single fuel-rich laminar premixed flames are convenient for studies of soot formation and have been widely used for this purpose. Such flames innately involve *soot-formation* paths and the flow/soot interactions that were just discussed are of little consequence; nevertheless, most experimental studies of the structure and soot-formation properties of fuel-rich premixed flames have involved measurements along the axes of the flames as a matter of convenience.

Early studies of flame structure and soot processes in laminar premixed flames are reviewed by Haynes and Wagner,[3] Glassman,[5] and Howard.[7] Other early studies of soot processes in laminar premixed flames, or in other configurations where effects of fuel/oxidant mixing are small, include Bockhorn and coworkers,[76-82] Harris and coworkers,[83-89] Ramer et al.,[90] Wagner and coworkers,[92-95] Howard and coworkers,[96-101] Macadam et al.,[102] Smedley et al.,[103] D'Alessio and coworkers,[104,105] and references cited therein. As a result of all these earlier studies, it was generally accepted that most of the mass of soot and associated heavy hydrocarbons came from acetylene, which generally is among the most abundant gaseous hydrocarbons in the region where soot is formed in laminar premixed flames. In addition, the reaction of acetylene to form soot was thought to occur in one of two ways: (1) by reactive addition of acetylene to growing and coalescing polycyclic aromatic hydrocarbons (PAH) that eventually either become soot nuclei or reactively coalesce at the surface of growing soot particles, and (2) by the direct reactive addition of acetylene to the surface of growing soot particles. Unfortunately, the results of the studies of Refs. 76-82 were unable to convincingly resolve the relative contributions of the two mechanisms to soot formation for given flame conditions, see Refs. 96-104. The early studies also found that soot particles became less reactive to soot growth with increasing residence time (age) in premixed flames. Frenklach and Wang[106] proposed that this reduced reactivity to soot growth was caused by reduced concentrations of H as flow temperatures decreased due to radiative heat losses from the flame to the surroundings because reactions between H and either the surface of soot particles or gaseous hydrocarbon molecules are needed to activate sites where carbon is added to either the carbon surface or the gaseous molecules. These features have been explained by Hydrogen-Abstraction/Carbon-Addition (HACA) processes developed by Frenklach and coworkers[101-110] and subsequently extended by others, e.g., Colket and Hall[111] and Mauss et al.[79] Unfortunately, there were concerns about the premixed laminar flame data base used to develop and evaluate the HACA models.[79,106-111] For example, residence times in the laminar premixed flames generally were only estimated rather than measured which compromises estimates of rate processes. In addition, soot structure was approximated by equivalent spherical particles, rather than treated as the aggregates of spherical primary soot particles that actually are observed in flame environments, which compromises estimates of important structural features of soot, e.g., surface-to-volume ratios.[20] Furthermore, approximations of the optical properties of soot by equivalent spherical particles have not been very effective, as already discussed.[11,23,24] Finally, the suite of measurements needed to completely define the soot growth environment of fuel-rich laminar premixed flames, required for even relatively simple HACA soot growth mechanisms, was not achieved during the earlier experimental studies of Refs. 76-111.

A series of investigations of soot formation in laminar premixed flames was undertaken by Xu and coworkers[112-114] seeking to remove some of the limitations of earlier studies about the structure and soot formation properties of fuel-rich laminar premixed flames. Test conditions involved fuel-rich laminar ethylene/air premixed flames similar to those considered by Harris and Weiner[83] and methane/oxygen flames similar to those considered by Ramer et al.[90] Measurements included soot volume fractions by both deconvoluted laser extinction and gravimetric methods, gas temperatures (where soot was absent) by corrected fine-wire thermocouples, gas temperatures (where soot was present) by deconvoluted multiline emission, soot structure by thermophoretic sampling and TEM, major gas species concentrations by sampling and gas chromatography, gas velocities by laser velocimetry, and radical (H, OH, O) species concentrations by the Li/LiOH technique in conjunction with deconvoluted atomic absorption to find the proportion of free lithium in the flames. These measurements were used to evaluate flame structure predictions in soot-containing flames based on the detailed chemical mechanisms of Frenklach and coworkers[106-110] and Leung and coworkers.[115,116] These predictions were obtained using PREMIX, the steady, laminar, one-dimensional premixed flame computer program of Kee et al.[117] In order to avoid the considerable uncertainties of heat loss predictions by conduction and radiation to the burner and by radiation to the surroundings, the measurements were used to prescribe temperature and velocity distributions as functions of distance from the burner exit. The measurements also were used to evaluate HACA soot growth theories due to Frenklach and coworkers[106-110] and Colket and Hall,[111] to evaluate soot oxidation models due to Nagle and Stickland-Constable[140] and Neoh et al.[141] and to test more simplified methods for treating soot nucleation; these applications of the measurements will be considered later.

Measurements of temperatures, velocities, soot volume fractions, primary soot particle diameters and the concentrations of major gas species along the axis of a laminar premixed ethylene/air flame having C/O = 0.88 at atmospheric pressure are plotted in Fig. 8. Corresponding residence times (relative to the first location where soot was observed), found by integrating the velocity measurements are shown at the top of the plot. These results are typical of the various laminar premixed flames studied by Xu and coworkers.[112-114]

Effects of buoyancy are significant for premixed flames at atmospheric pressure so that streamwise velocities in Fig. 8 rapidly increase from burner exit values of roughly 70 mm/s to values of roughly 1 m/s at the highest position where measurements were made. The presence of soot causes significant radiative heat losses so that soot temperatures decrease from 1900-2100 K near z = 7.5 mm to values of 1500-1600 K at the highest location measured (z = 27.5 mm). The optical determinations of soot volume fractions were in good agreement with gravimetric measurements and with optical measurements of Benish et al.[100] for similar flames; in contrast, the results of Harris and Weiner[83] are nearly three times larger in similar flames, for reasons that have not been explained. Finite soot volume fractions are first observed near z = 7.5 mm, and then soot volume fractions substantially increase before leveling off near the highest position where measurements were made (which is typical of past observations in premixed soot-containing flames[3,83]). Mean primary soot particle diameters increase and then level off with increasing distance from the burner exit similar to soot volume fractions. Concentrations of major gas species agree with Harris and Weiner[83] and Benish et al.[100] where they overlap for similar flame conditions. The concentrations of major gas species are nearly constant throughout the soot formation region, similar to the findings of Harris and Weiner.[83] This includes potential soot-forming hydrocarbons, e.g., acetylene, which suggests that soot formation does not decrease due to consumption of fuel-like materials which is the case for laminar diffusion flames.[59,60,68]

It is evident from Fig. 8 that concentrations of major gas species exhibit little variation with distance within the soot formation region of the present flames. On the other hand, it is of interest to examine the yields of major gas species as a function of C/O ratio because this highlights the gas species responsible for the growth and nucleation of soot. Thus, measured

concentrations of major gas species for the premixed ethylene/air flames are plotted as a function of C/O ratio, in Fig. 9. Predictions of these properties based on the mechanisms of Frenklach and coworkers[106-110] (250 reversible reactions and 52 species involving hydrocarbons up to benzene) and Leung and Lindstedt[116] (451 reversible reactions involving 87 species up to benzene) are also shown on the plot. Both measurements and predictions are for z = 20 mm but effects of distance on major species concentrations were small as discussed in connection with Fig. 8. Harris and Weiner[83] report concentrations of acetylene and methane in similar flames that are in good agreement with the results of Fig. 9; these results suggest that acetylene is the dominant light hydrocarbon species that is likely to contribute to soot formation. Predictions using the two mechanisms are essentially the same and are in good agreement with the measurements; predictions of yields of major gas species for methane/oxygen flames were similarly in good agreement with measurements.[113,114]

In view of the good predictions of major gas species concentrations in the premixed ethylene/air and methane/oxygen flames, evaluation of the predictions was extended to consider concentrations of the H-radical which is an important species for the HACA soot growth mechanism. Results of this evaluation for premixed methane/oxygen flames are illustrated in Fig. 10, considering results for premixed flames having fuel-equivalence ratios of 2.45, 2.56 and 2.67. For each flame, the mole fraction of H is plotted as a function of distance from the burner exit, considering four ways of finding the concentration of H, as follows: (1) direct measurements using the Li/LiOH technique in conjunction with deconvoluted atomic absorption to find the proportion of free lithium; (2) estimated using predictions based on the mechanism of Frenklach and coworkers,[106-110] (3) estimated using predictions based on the mechanism of Leung and Lindstedt,[116] and (4) estimated based on the assumption of local thermodynamic equilibrium of H from the thermochemical properties of Chase et al.[118] and present measurements of H_2 concentrations and temperatures. Similar to all the premixed flames considered by Xu and coworkers,[112-114] predictions of H concentrations using the mechanisms of Frenklach and coworkers[106-110] and Leung and Lindstedt,[116] are in good agreement with each other and are in excellent agreement with estimates based on the assumption of local thermodynamic equilibrium. Finally, all the estimates are in excellent agreement with the direct measurements of H concentrations. This behavior is not surprising because changes of flame properties are relatively slow, and effects of streamwise diffusion are relatively small, in the soot formation regions of premixed flames so that it is not difficult for thermodynamic equilibrium to be maintained. This helps explain the termination of soot formation as a result of reduced H concentrations with increasing streamwise distance through the HACA mechanism (soot growth rates are roughly proportional to the concentration of H in the HACA mechanism). In turn, H concentrations decrease due to reduced temperatures through the requirement of local thermodynamic equilibrium. Finally, temperatures decrease due to radiative heat losses that are dominated by continuum radiation from soot for these conditions; therefore, the formation of soot itself serves to limit the amount of soot that can form in laminar premixed flames. It will be shown later that the HACA mechanism provides a quantitative prediction of soot growth rates in these flames; thus, soot growth ends in premixed flames directly due to reduction of H concentrations as suggested by Frenklach and coworkers[106] so that there is no need to hypothesize effects of soot aging on soot growth that was done during early studies of soot growth in laminar premixed flames, see Refs. 2 and 3.

It seems very encouraging to achieve good predictions of the yields of major gas species and the behavior of H concentrations in soot-containing laminar premixed flames. When interpreting this finding, however, two limitations of these results should be kept in mind: (1) yields of major gas species mainly result from processes in the flames before the appearance of any soot (generally at z < 5 mm) for the results of Xu and coworkers[112-114], and (2) maximum soot concentrations in any of the premixed flames studied by Xu and coworkers[112-114] were never very large (e.g., maximum concentrations of soot generally

were smaller than 0.02% of the mass of carbon in the reactants for the test flames).[114] It is this latter condition that is responsible for the negligible variation of hydrocarbon species concentrations in the region of soot growth that is seen in Fig. 8. More definitive evaluation of methods of predicting the structure of soot-containing flames should be possible considering nonpremixed flames, however, which will be discussed next.

Structure of Nonpremixed Soot-Containing Flames

Soot processes in nonpremixed (diffusion) flames are of critical importance because practical soot formation processes generally occur within diffusion flames. Measurements and analysis of soot processes in laminar diffusion flames have considered a variety of conditions: flames around drops or analogous spherical gaseous diffusion flames,[5,75] opposed-jet diffusion flames,[119,120] and jet or coflowing jet diffusion flames,[8,58-65] These configurations involve a variety of flame conditions under the designation of Kang et al.,[70] e.g., *soot formation* paths and *soot-formation-oxidation* paths. As discussed earlier with respect to soot/flow interactions, laminar jet diffusion flames provide a good qualitative simulation of *soot-formation-oxidation* paths of most practical applications, for measurements along the axis; therefore, studies using this configuration will be emphasized in the following.

Early studies of the structure and soot processes of soot-containing laminar jet diffusion flames are reviewed by Haynes and Wagner,[3] Glassman,[5,6] and Kennedy.[8] More recent studies of the structure and soot processes of soot-containing laminar jet diffusion flames include Samson et al.[19] Urban et al.,[21,22,73] Dobbins and coworkers,[31-33] Vander Wal,[34-36] Megaridis and Dobbins,[39] Puri et al.,[44,64,65,121,122] Sunderland and coworkers,[58-60,72] Lin and Faeth,[61,71] Santoro and coworkers,[62,63,120] Xu and coworkers,[68,69,135] Balthasar et al.,[81] Garo et al.,[122,123] Hardiquert et al.,[124] Mitchell et al.,[125] Smooke and coworkers,[126-133] Saito et al.,[134] McEnally and coworkers,[135-138] and references cited therein. Of these studies, the recent investigations of Xu and coworkers,[58,59,139] provide the most complete information about the structure and soot reaction properties of soot-containing laminar jet diffusion flames and will be considered in the following. Test conditions involved round soot containing laminar coflowing jet diffusion flames fueled with acetylene, ethylene, propylene and propane and burning in air at atmospheric pressure. Fuels having a large propensity to soot, e.g., acetylene and propylene, were diluted with nitrogen so that maximum soot concentrations were less than 1 ppm in order to avoid measurement problems caused by excessive amounts of soot. Measurements in these flames were the same as those of Xu and coworkers[112-114] for laminar premixed flames: soot volume fractions by deconvoluted laser extinction, gas temperatures (where soot was present) by deconvoluted multiline emission, soot structure by thermophoretic sampling and TEM, major gas species concentrations by sampling and gas chromatography, gas velocities by laser velocimetry, and radical (H, OH, O) species concentrations by the Li/LiOH technique in conjunction with deconvoluted atomic absorption to find the proportion of free lithium in the flames. These measurements were used directly to gain a better understanding about the environment of soot processes in diffusion flames. The measurements also were used to evaluate soot reaction processes, e.g., HACA soot growth theories due to Frenklach and coworkers[106-110] and Colket and Hall,[111] to evaluate soot oxidation theories due to Nagle and Strickland-Constable[140] and Neoh et al.,[27,141] and to qualitatively consider ways to correlate soot nucleation theories. Soot reaction properties, however, will be considered in later sections of the paper.

Measurements of gas (soot) temperatures, streamwise gas velocities, soot volume fractions, soot primary particle diameters, the concentrations of major gas species and the concentrations of radical (H, OH, O) species are plotted a function of height above the burner for conditions along the axis of an acetylene/air diffusion flame (burner flow of 15.1% acetylene-by-volume in nitrogen) at atmospheric pressure in Fig. 11. Corresponding residence times, found by integrating the velocity measurements, are indicated at the top of the plot. The residence times were used to find soot reaction rates and are relative to the first position where

detectable soot volume fractions were observed (at roughly z = 10 mm). The composition measurements showed that these observations were entirely at fuel-rich conditions (with fuel-equivalence ratios greater than 1.10). Noting that the soot forms and oxidizes completely over the region of these measurements, it is clear that substantial levels of soot oxidation occur at fuel-rich conditions even though concentrations of O_2 are relatively small.

Gas (soot) temperatures along the axis reach a maximum well before regions of greatest soot production and the flame sheet (the condition where the fuel-equivalence ratio is unity which is downstream of the region where measurements were made) in Fig. 11. The maximum temperature is also significantly smaller than the adiabatic combustion temperature of the reactant mixture of this flame (2320 K).[68] These trends are qualitatively similar to the earlier observations of Sunderland et al.[59] of acetylene-fueled laminar coflowing jet diffusion flames burning in air at subatmospheric pressures. This behavior is caused by significant effects of continuum radiation from soot[53,60] with potential contributing effects of preferential diffusion for species and heat.

Streamwise velocities illustrated in Fig. 11 increase from burner exit values of roughly 30 mm/s to values in excess of 2 m/s at the highest position that was measured. This is the result of significant effects of buoyancy for these test conditions, which is typical of laminar flames at atmospheric pressure.

The primary soot particle diameters plotted in Fig. 11 reach maximum values relatively early in the soot formation region, well before conditions where maximum soot volume fractions are reached, relatively similar to earlier observations in the soot formation regions of laminar diffusion flames, see Refs. 59 and 60. This behavior is caused by accelerating soot nucleation rates with increasing streamwise distance. This causes the relatively few primary particles formed near soot inception conditions (the first location where soot is formed along the flame axis), that become large due to lengthy periods of soot growth, to be superseded by large numbers of primary soot particles formed later in the soot formation region, that are smaller due to smaller residence times for soot growth. Notably, Tesner[142,143] has observed that soot growth remains relatively rapid at soot inception conditions where soot nucleation rates are small, which is consistent with the primary particle diameter behavior seen in Fig. 11.

Significant levels of soot formation, based on increasing values of soot volume fractions in the streamwise direction, were generally associated with the first location along the flame axis where detectable concentrations of H were observed, e.g., where H mole fractions exceeded 10^{-5}. The subsequent soot formation region, however, contains significant concentrations of species potentially responsible for soot oxidation, e.g., O_2, CO_2, H_2O, O and OH.[140,141,144-156] Thus, soot formation and oxidation proceed at the same time with soot formation dominating the process up to the maximum soot volume position and soot oxidation dominating the process thereafter. The maximum soot volume fraction condition is reached where concentrations of acetylene become small (e.g., where acetylene mole fractions are less than 1%) which is well before the flame sheet, similar to earlier observations of Sunderland et al.[59] within acetylene-nitrogen diffusion flames burning in air. Thus, unlike premixed flames where soot growth ends when H concentrations become small with substantial concentrations of acetylene remaining and effects of soot oxidation are negligible; in diffusion flames, soot growth ends when acetylene concentrations become small with substantial concentrations of H remaining and in the presence of significant effects of soot oxidation. Finally, effects of soot oxidation clearly are very significant in the fuel-rich region of diffusion flames (the only region illustrated in Fig. 11), e.g., they are sufficient to completely oxidize all the soot formed in the acetylene/air flame illustrated in Fig. 11. The results illustrated in Fig. 11 are typical of all the other flames considered by Xu and coworkers,[114,139] which includes acetylene, ethylene, propylene and propane burning in air at atmospheric pressure with nitrogen dilution used to keep maximum soot concentrations smaller than 1 ppm: fuels other than acetylene decompose to yield acetylene near the burner exit so that acetylene appears to be the

dominant hydrocarbon involved in the formation of soot, the end of soot growth generally coincides with concentrations of acetylene becoming small in the presence of significant concentrations of H, and soot oxidation at fuel-rich conditions is significant — sufficient to completely oxidize all the soot that is formed in the region where acetylene is present.

The relationship between soot concentrations and primary soot particle diameters is complex for the conditions illustrated in Fig. 11 and in other diffusion flames that have been observed, see Refs. 59, 60, 68 and 139, due to varying soot nucleation, growth and oxidation rates. Thus, soot primary particle diameters reach a maximum well before soot volume fractions reach a maximum, with the intervening region involving a large increase in the number of primary particles per unit volume.

The concentrations of major stable gas species in Fig. 11 are in qualitative agreement with earlier measurements in acetylene-nitrogen/air diffusion flames due to Sunderland et al.[59] Acetylene and O_2 decrease and increase monotonically, respectively, throughout the soot formation region, whereas the intermediate hydrocarbons, methane and ethylene, reach maxima roughly when primary soot particle diameters reach maxima. When other hydrocarbons are used instead of acetylene (e.g., ethylene, propylene and propane) the fuel hydrocarbon concentration decreases monotonically similar to acetylene in Fig. 11, whereas acetylene plays the role of an intermediate hydrocarbon and maintains large concentrations in the soot growth region (fuel decomposition is rapid, however, so that variations of hydrocarbon concentrations are qualitatively similar to Fig. 11).[139] The final combustion products increase throughout the soot formation region, finally reaching broad maxima near the flame sheet (ϕ=1). The intermediate combustion products associated with water-gas equilibrium, H_2 and CO, both are present in relatively large concentrations throughout the soot formation region, reaching broad maxima somewhat upstream of the flame sheet. Finally, nitrogen concentrations at the burner exit are comparable to nitrogen concentrations in the ambient air for the conditions of Fig. 11; therefore, nitrogen concentrations are relatively constant for the flame illustrated in Fig. 11.

The Li/LiOH atomic absorption technique yields concentrations of H, OH and O.[68,114,141] These measurements were compared with equilibrium estimates of these radical concentrations that were found using the equilibrium data base of Chase et al.[118] and the measured temperatures and stable major gas species concentrations in the flames. The resulting superequilibrium ratios of H, O and OH are plotted as a function of distance from the burner exit in Fig. 12 for the acetylene-fueled laminar diffusion flames burning in air at atmospheric pressure (these results are for conditions at the flame axis with flames 1, 2 and 3 having acetylene concentrations in nitrogen at the burner exit of 16.9, 15.1 and 17.1 percent by volume, respectively). The superequilibrium ratios progressively increase with increasing streamwise distance approaching values in excess of 10 for H and OH and values in excess of 100 for O as the flame sheet is approached. Thus, as noted earlier, unlike laminar premixed flames where soot growth ends where H concentrations become small, soot formation ends in diffusion flames in the presence of significant concentrations of H and the end of growth mainly occurs where acetylene concentrations become small.

Soot Reaction Rate Properties

Measurements in both premixed and diffusion flames due to Xu and coworkers[68,69,112,113,139] were used to study soot growth, oxidation and nucleation. Major assumptions made when reducing the data were identical to earlier work by Sunderland and coworkers:[59,60] soot surface growth, rather than soot nucleation, dominates soot mass production; effects of diffusion (Brownian motion) and thermophoresis on soot motion are small, so that soot particles convect along the flame axis at the local gas velocity; the soot density is constant (1850 kg/cu-m); and the surface area available for soot growth is equivalent to constant diameter primary soot particles that meet at a point, see Refs. 59, 60, 68, 69, 112, 113 and 139 for justification of these assumptions.

Soot structure properties that are needed to find soot reaction rate properties

include the number of primary particles per unit volume and the soot surface area for unit volume. These were found according to Sunderland et al.,[59] as follows:

$$n_p = 6f_s/(\pi a_p^3) \quad (2)$$

and

$$S = 6f_s/d_p \quad (3)$$

Then defining soot growth rate as the rate of increase of soot mass per unit soot surface area and time, conservation of soot mass along a streamline under the previous assumptions yields:[59]

$$w_g = (\rho/S)d(\rho_s f_s/\rho)dt \quad (4)$$

Finally, soot nucleation was defined as the rate of increase of the number of primary particles per unit volume and time. Under the previous assumptions, this becomes:[59]

$$w_n = \rho d(n_p/\rho)dt \quad (5)$$

All qualities needed to find n_p, S, w_g and w_n are known from direct measurements, as discussed by Sunderland et al.[59]

The four derived soot reaction rate properties are plotted as functions of distance along the axes of the three acetylene/air diffusion flames in Fig. 13. As before, Flames 1, 2 and 3 have 16.9, 15.1 and 17.5 percent by volume of acetylene in nitrogen at the burner exit. Similar results for ethylene, propylene and propane fueled diffusion flames can be found in El-Leathy et al.,[139] whereas similar measurements for laminar premixed flames can be found in Xu et al.[112,113]

The soot surface area per unit volume tends to vary similar to the soot volume fraction, increasing within the soot formation region until the soot volume fraction reaches a maximum and then decreasing once again in the soot oxidation region. Values of the number of primary particles per unit volume increase substantially from conditions where the primary soot particle diameter reaches a maximum at z = 30-40 mm to conditions where the soot volume fraction reaches a maximum at z = 50-60 mm. This substantiates the earlier discussion of the way that rapid nucleation is responsible for decreases of d_p as f_s increases in the soot growth region. Soot nucleation rates vary with streamwise distance in qualitatively the same way as growth rates, except that there is a delay in reaching maximum values. The variation of soot nucleation rates is much larger than the variation of soot growth rates over the range of the measurements: three orders of magnitude for soot nucleation rates compared to roughly one order of magnitude for soot growth rates. This helps explain the anomalous reductions of soot primary particle diameters as soot volume fraction increases, as discussed earlier.

Soot Surface Growth

Gross soot growth rates obtained from Eq. 4 were corrected for effects of soot oxidation in a unified way for the measurements of Sunderland and coworkers[59,60] and Xu and coworkers.[68,112,113,149] During the period of these studies, there was considerable uncertainty about soot oxidation rates in flame environments, as will be discussed in the next section. Thus, considerations of soot growth were limited to conditions where estimated soot oxidation rates never exceeded half the soot growth rates using methods that give a high estimate of the oxidation rate (data on growth in the following all have negligible oxidation corrections but some good data points probably were discarded using this approach). Soot oxidation was estimated as follows: soot oxidation by O_2 was based on the results of Nagle and Strickland-Constable,[140] soot oxidation by H_2O and CO_2 was estimated following Libby and Blake[153,154] and Johnstone et al.,[155] which gives results similar to Bradley et al.,[156] and soot oxidation by O and OH was ignored.

Soot surface growth rates using the HACA mechanisms of Frenklach and coworkers[106-110] and Colket and Hall[111] have been evaluated using the data base for laminar premixed and diffusion flames developed by Xu and coworkers.[68,112,113,139] The net rate of soot surface growth was expressed as follows for both mechanisms:

$$w_g = \alpha_i R_i \quad (6)$$

where i = FW or CH denotes the appropriate reaction parameters for the mechanisms of Frenklach and coworkers[106-110] and Colket and Hall.[111] The details of these mechanisms, the formulas for the R_i, and the reaction rate parameters appearing in the expressions for the R_i can be found in Xu et al.[112] The parameters, α_i, are steric factors on the order of unity, with α_{FW} specified to be a function of temperature,[106-111] and α_{CH} specified to be a constant.[111] The correlation for α_{FW} over the

entire data base is presented in El-Leathy, et al.[139] and will not be considered here; the values of $\alpha_{CH} = 0.9$ over the same data base.

The R_i for the HACA mechanism of Frenklach and coworkers[106-110] and of Colket and Hall[111] are proportional to $[H][C_2H_2]$as a first approximation for both laminar premixed and diffusion flame environments. Thus, $w_g/[C_2H_2]$ for the studies of Xu and coworkers.[69,112,113] are plotted as a function of [H] in Fig. 14 in order to provide a direct test of the main features of the HACA soot growth mechanisms without the intrusion of uncertainties in the original detailed mechanisms of Frenklach and coworkers[106-110] and Colket and Hall.[111] The correlation of the results for both premixed and diffusion flames according to the approximate HACA mechanism is remarkably good, showing that soot surface growth in premixed and diffusion flames is consistent in spite of substantial fundamental differences between their soot formation environments. Finally, the strong effect of [H] on w_g, combined with near-equilibrium and strongly superequilibrium behavior of [H] in premixed and diffusion flames, respectively, clearly is responsible for the enhanced soot growth rates in diffusion flames compared to premixed flames at comparable acetylene concentrations and temperatures that were reported by Sunderland and coworkers[59,60]

A more direct evaluation of the Colket and Hall[111] HACA mechanism for soot surface growth is obtained by plotting w_g directly as a function of R_i for the laminar premixed and diffusion flames as illustrated in Fig. 15. The measurements are seen to be in good agreement with the best-fit correlation which clearly is effective for both premixed and diffusion flames.

The evaluation of HACA soot growth mechanisms of Frenklach and coworkers[106-110] and Colket and Hall[111] are very encouraging and these approaches may eventually provide robust methods to estimate soot growth rates in flame environments. Uncertainties remain, however, about the behavior of soot growth in flames (particularly diffusion flames) fueled by hydrocarbons other than the simple fuels considered thus far (methane, ethylene, acetylene, propylene, and propane) about effects of pressures on soot growth and about the relative contributions of the HACA and PAH mechanisms to soot growth discussed by Howard,[7] particularly when the fuel involves PAH compounds.

Soot Surface Oxidation

Potential soot oxidants include O_2, CO_2, H_2O and OH. Numerous simplified treatments have been reported that can be used to estimate soot oxidation rates in frequently-encountered instances when local radical concentrations are not known, see Revs. 140, 144 and 153-156. Even though these procedures were used during the studies of soot growth of Sunderland and coworkers[59-60] and Xu and coworkers,[69,112,113,149] a more fundamental approach that includes potential contributions of both stable and radical species is needed to provide a reasonably robust approach useful for future estimates of soot oxidation in practical flames. Thus, recent progress toward developing such methods is discussed in the following.

The results of the classical study of the oxidation of pyrolytic graphite by O_2 due to Nagle and Strickland-Constable,[140] have been shown to be effective for soot oxidation by O_2 as well, based on later work by Radcliffe and Appleton[144] and Park and Appleton.[145] Subsequent work by Fenimore and Jones[148] and Mulcahy and Young,[149] however, showed that soot oxidation rates in flame environments having relatively small O_2 concentrations substantially exceeded estimates based on the results of Nagle and Strickland-Constable,[140] prompting suggestions that radicals such as O and OH might be strong contributors to soot oxidation for such conditions. Neoh and coworkers[27,141] subsequently observed soot oxidation in premixed flames and found that OH was the principle oxidant of soot for near-stoichiometric flame conditions (with O_2 mole fractions smaller than 5 percent), they also found an OH collision efficiency of 0.13 for soot oxidation where accounting for the actual structure of soot particles as aggregates of primary particles. Later studies of Wicke and coworkers[150,151] and Roth et al.[152] confirmed the findings of Neoh and coworkers.[27,141]

Due to the importance of soot processes within diffusion flames, there have been several recent investigations of soot oxidation in laminar diffusion flames. This

has included measurements of soot oxidation in round methane/air coflowing jet diffusion flames due to Garo et al.,[122,123] in round ethylene/air coflowing jet diffusion flames due to Puri et al.,[65,157] and in ethylene-nitrogen/oxygen-argon Wolfhard-Parker burner flames due to Haudiquert et al.[124] These studies supported the important role of OH in the mechanism of soot oxidation within diffusion flames, however, observations of OH collision efficiencies for soot were not in good agreement with the earlier results for premixed flames, e.g., Garo et al.,[122,123] observed values of 0.012-0.094 that generally *increased* with increasing temperature, Puri et al.,[65,157] observed values of 0.03-0.15 that generally *decreased* with increasing temperature and Haudiquert et al.[124] observed values of 0.01-0.11 that generally *decreased* with increasing temperature. One explanation for these discrepancies is that optical scattering and extinction measurements were used to find soot structure properties during these studies based on models that have not been very successful for representing the optical properties of soot.[10,20] In particular, use of similar methods during early studies of soot growth in premixed flames also proved to be problematical, see Xu and coworkers.[112,113]

In an attempt to resolve the discrepancies among the collision efficiencies for soot oxidation by OH in diffusion flame environments Xu et al.[69] undertook an investigation of soot oxidation in coflowing laminar jet diffusion flames burning in air at atmospheric pressure. The particular hydrocarbon fuels considered during this study included those used by Sunderland and coworkers[59-60] One limitation of this work, however, was that only the early stages of soot oxidation were considered (carbon mass consumption less than 70%) where reaction at the surface of primary soot particles dominates the process, rather than the later stages where particle porosity and internal oxidation of the particles become important, as discussed by Neoh et al.[27] Experimental methods were identical to the studies of Xu et al.,[68,139] of soot growth in laminar flames: soot volume fractions were measured by deconvoluted laser extinction, gas temperatures (when soot was present) were measured by deconvoluted multiline emission, soot structure was measured by thermophoretic sampling and TEM, major gas species concentrations were measured by sampling and gas chromatography, gas velocities were measured by laser velocimetry, and radical (H, OH, O) species concentrations were measured by the Li/LiOH technique in conjunction with deconvoluted atomic absorption to find the proportion of free lithium in the flames. Soot oxidation rates were found as discussed in connection with Eqs. 2-4, with the following expression specifically used to find the soot oxidation rate per unit surface area:

$$w_{ox} = -(\rho/S)d(\rho_s f_s/\rho)dt \qquad (7)$$

where the minus sign is inserted so that w_{ox} is a positive number. The measurements were limited to the soot oxidation region so that effects of soot growth were small; nevertheless, the measurements were corrected for effects of soot growth using the expression based on Colket and Hall[111] as corrected for both premixed and diffusion flame environments by Xu and coworkers.[69,112,113,139] see Fig. 15 for an indication of the fit of the correlation for typical laminar flame conditions. No condition was considered, however, where the correction for soot growth was more than half the soot oxidation rate. Thus, the correction of soot oxidation rates for soot growth was analogous to the earlier correction of soot growth rates for effects of soot oxidation: the correction mainly served to narrow the acceptable test range and did not strongly affect the oxidation rate values that were reported.

Following Neoh and coworkers,[27,141] the soot oxidation rates corrected for soot growth were converted into collision efficiencies (or reaction probabilities) based on kinetic theory estimates of the collision rates of a given gas species with the surfaces of primary soot particles. Thus, the collision efficiency of a potential oxidizing species, i, is given by the following expression:[60]

$$\eta_i = 4w_{ox}/(C_i[i]\bar{v}_i) \qquad (8$$

where C_i is the mass of carbon removed from the surface per mole of species i reacting at the surface, [i] is the gas phase concentration of i adjacent to the surface, and

$$\bar{v}_i = (8kT/(\pi M_i))^{1/2} \qquad (9$$

is the (Boltzmann) equilibrium mean molecular velocity of species i.

Typical measurements of flame structure and reaction properties for the soot oxidation study of Xu et al.,[69] were the same as for the studies of soot growth due to Xu and coworkers[68,139] and have already been discussed in connection with Figs. 11-13. The entire suite of measurements were used to find collision efficiencies for potential soot oxidation by O_2, CO_2, H_2O, O and OH; the following will be limited to results for O_2 and OH, see Xu et al.[69] for the complete results.

The collision efficiencies of O_2 for soot oxidation are plotted as a function of height above the burner in Fig. 16. The results shown on the figure include the range of values observed by Neoh et al.[121] in premixed flames, values estimated from the predictions of Nagle and Strickland-Constable,[140] for the conditions in diffusion flames, and values from the measurements of Xu et al.[69] for the diffusion flames. Now, the Nagle and Strickland-Constable[140] approach has exhibited effective capabilities to predict soot oxidation by O_2 when O_2 is the only oxidizer species in the environment and there are significant levels of O_2 soot oxidation region of the test flames, see Fig. 11. Then, the fact that the Nagle and Strickland-Constable[140] estimates of the O_2 collision efficiency are 10-100 times smaller than the measurements in Fig. 16 strongly suggests that some other species is mainly responsible for soot oxidation in the present flames. Other evidence that O_2 is not the main direct soot oxidizing species for flame environment is provided by the large scatter (nearly a factor of 100) of the collision efficiencies for the diffusion flames considered in Fig. 16 with the even larger scatter (more than a factor of 100) of the O_2 collision efficiencies of Neoh and coworkers[141] in premixed flames. Evaluations of the collision efficiencies for CO_2, H_2O and O for these conditions lead to similar results: collision efficiencies for premixed flames from Neoh et al.[141] and those for diffusion flames from Xu et al.[69] were both badly scattered. In addition, small O concentrations also required collision efficiencies greater than unity in order to explain measured soot oxidation rates which clearly is not possible.

Finally, the collision efficiencies of OH for soot oxidation in various premixed and diffusion flames are plotted as a function of distance from the burner in Fig. 17. Two measurements are illustrated for each flame condition for the results of Xu et al.:[69] one considering the contribution to oxidation by O_2 (estimated using the Nagle and Strickland-Constable[140] correlation) and one assuming that oxidation was entirely due to OH. With perhaps one exception, direct oxidation of soot by O_2 was not very important for the diffusion flames. On the other hand, similar to the observations of Neoh et al.[141] for premixed flames, the collision efficiencies of OH for the diffusion flames exhibit relatively small levels of scatter (roughly a factor of 3). Furthermore, the results for the premixed and diffusion flames are in remarkably good agreement with each other. Taken together, the collision efficiency for soot oxidation by OH, allowing for direct oxidation of soot by O_2 using the Nagle and Strickland-Constable[140] correlation, is 0.10. This result was determined for a broad range of flame conditions considering both premixed and diffusion flames, as follows: temperatures of 1570-1870 K, oxygen mole fractions of $1 \times 10^{-5} - 1.2 \times 10^{-2}$ and levels of soot mass consumption less than 70% at atmospheric pressure. While these results are helpful, however, the properties of the final stage of soot oxidation (where internal oxidation of primary particles becomes a factor), effects of pressure on soot oxidation, the transition between OH-dominated and O_2-dominated soot oxidation in high-temperature environments, and possibly effects of fuel type on soot oxidation for hydrocarbons (other than those considered thus far) all merit additional study in the future.

Another area where more work is needed is that past studies of soot growth in premixed and diffusion flames should be reconsidered in order to update the estimates of soot oxidation to the combined OH and O_2 mechanisms from the approach based on stable gas species, e.g., O_2, CO_2 and H_2O along the lines considered by Sunderland and coworkers[59,60] and Xu and coworkers.[69,112,113,139] Notably, preliminary work along these lines indicates negligible changes of reported soot growth rates but final resolution of this issue certainly is needed.

Soot Nucleation

Soot nucleation is complex and involves processes analogous to soot surface growth in order to form large molecular weight soot precursor species, processes of coagulation of large molecules to form soot nucleation sites, and processes of dehydrogeneration of coagulated soot precursor species in order to reach carbon concentrations typical of primary soot particles, among others. This has lead to a large number of simplified models discussed by Kennedy[8] that provide estimates of soot nucleation rates as a function of stable species concentrations and temperatures. Thus, the following discussion is limited to more recent work which seeks to develop more detailed, and thus potentially more robust, methods of predicting soot nucleation rates.

A recent approach toward achieving a model of soot nucleation is an approximate model due to Xu and Faeth.[68] The main hypothesis made in this model is that soot nucleation is dominated by large molecular weight soot precursor species whose rates of formation should be similar to soot surface growth. For example, the study of Stein and Fahr[152] finds that certain species are likely to appear during soot growth due to their relative stability in high temperature gases (thus, they are called *stabilomers*) include PAH molecules. On the other hand, the HACA soot growth mechanisms are modeled on growth rates of PAH molecules so that a reaction rates in both cases are related. In addition, past work finds soot nucleation rates proportional to acetylene concentrations which tends to support this behavior because acetylene is a leading term in the HACA soot growth mechanisms as discussed in connection with Fig. 14.[59,60,68,112,113] Finally, plots of normalized soot nucleation rates, $w_n/[C_2H_2]$, as a function of [H], yielded results comparable to this for soot growth illustrated in Fig. 14. Based on these observations a simplified correlation was attempted in terms of acetylene and H concentrations, and the temperature, as follows:

$$w_n = k_n(T)[C_2H_2][H] \qquad (10)$$

where a correlation of $k_n(T)$ was sought in terms of an Arrhenius expression.

Based on Eq. 10, available primary soot particle nucleation rates are plotted in Fig. 18 as $k_n = w_n/([C_2H_2][H])$ as a function of reciprocal temperature in order to assess an Arrhenius correlation of this function. Results for both premixed and diffusion flames are consistent when plotted in this way. This behavior shows that superequilibrium and near-equilibrium H concentrations for diffusion and premixed flames, respectively, are responsible for the much larger rates of soot nucleation observed in diffusion flames than in premixed flames at comparable temperatures and acetylene concentrations.[59,60] Furthermore, the apparent negative activation energy is similar to the behavior of the HACA mechanisms of Frenklach and coworkers[106-110] for soot growth which has similar dominant variables, e.g., [H] and $[C_2H_2]$. Achieving some merging of primary particle nucleation rates in premixed and diffusion flames, as seen in Fig. 18, represents a step toward a more satisfactory treatment of soot nucleation. Improved models of this process, however, that achieve less scattered results, and which properly account for the detailed chemical and physical processes responsible for soot nucleation, clearly are needed. Furthermore, a computationally-tractable and robust treatment of soot nucleation, growth and oxidation has not yet been achieved, e.g., even the somewhat successful soot growth and oxidation models discussed here require accurate estimates of radical concentrations that are by no means assured in practical soot-containing diffusion flame environments. Until these limitations have been resolved, recommendations concerning predictions of the rates of soot formation and oxidation in practical flames still must be confined to the simplified empirical approaches discussed by Kennedy.[8]

Acknowledgments

This work was supported by the National Aeronautics and Space Administration under NASA Grants NAG3-1245 and NAG3-2048.

References

[1]Palmer, H.B., and Cullis, H.F., "The Formation of Carbon from Gases," *The Chemistry and Physics of Carbon*, Marcel Dekker, New York, Vol. 1, 1965, pp. 265-325.

[2]Wagner, H. Gg., "Soot Formation in Combustion," *Proceedings of the Combustion Institute*, Vol. 17, 1978, pp. 3-19.

[3]Haynes, B. S., and Wagner, H. G., "Soot Formation," *Progress in Energy and Combustion Science*, Vol. 7, No. 4, 1981, pp. 229-273.

[4]Donnet, J.B., "Structure and Reactivity of Carbons: from Carbon Black to Carbon Composites," *Carbon*, Vol. 20, No. 4, 1982, pp. 266-282.

[5]Glassman, I., "Soot Formation in Combustion Processes," *Proceedings of the Combustion Institute*, Vol. 22, 1988, pp. 295-311.

[6]Glassman, I., "Sooting Laminar Diffusion Flames: Effect of Dilution, Additives, Pressure and Microgravity," *Proceedings of the Combustion Institute*, Vol. 22, 1998, pp. 1589-1596.

[7]Howard, J.B., "Carbon Addition and Oxidation Reactions in Heterogeneous Combustion and Soot Formation," *Proceedings of the Combustion Institute,* Vol. 23, 1990, pp. 1107-1127.

[8]Kennedy, I.M., "Models of Soot Formation and Oxidation," *Progress in Energy and Combustion Science*, Vol. 23, No. 2, 1997, pp. 95-132.

[9]Jullien, R., and Botet, R., *Aggregation and Fractal Aggregates*, World Scientific Publishing Co., Singapore, 1987, pp. 45-60.

[10]Köylü, Ü.Ö., and Faeth, G.M., "Radiative Properties of Flame-Generated Soot," *Journal of Heat Transfer,* Vol. 115, No. 2, 1993, pp. 409-417.

[11]Faeth, G.M., and Köylü, Ü.Ö., "Soot Morphology and Optical Properties of Nonpremixed Turbulent Flame-Environments," *Combustion Science and Technology,* Vol. 108, Nos. 4-6, 1995, pp. 207-229.

[12]Alden, M., "Laser Spectroscopic Techniques for Combustion Diagnostics," *Combustion Science and Technology*, Vol. 149, Nos. 1-6, 1999, pp. 1-18.

[13]Dalzell, W.H., Williams, G.C., and Hottel, H.C., "A Light Scattering Method for Soot Concentration Measurements," *Combustion and Flame,* Vol. 14, No. , 1970, pp. 161-170.

[14]Dobbins, R.A., and Megaridis, C.M., "Morphology of Flame-Generated Soot as Determined by Thermophoretic Sampling," *Langmuir*, Vol. 3, No. 2, 1987, pp. 254-259.

[15]Erickson, W.D., Williams, G.C., and Hottel, H.C., "Light Scattering Measurements on Soot in a Benzene-Air Flame," *Combustion and Flame,* Vol. 8, No. 2, 1964, pp. 127-132.

[16]Köylü, Ü.Ö., and Faeth, G.M., "Structure of Overfire Soot in Buoyant Turbulent Diffusion Flames at Long Residence Times," *Combustion and Flame,* Vol. 89, No. 2, 1992, pp. 140-156.

[17]Medalia, A.I., and Heckman, F.A., "Morphology of Aggregates — II. Size and Shape Factors of Carbon Black Aggregates from Electron Microscopy," *Carbon,* Vol. 7, 1969, pp. 567-582.

[18]Nelson, J., "Test of a Mean Field Theory for the Optics of Fractal Clusters," *Journal of Modern Optics,* Vol. 36, 1989, pp. 1031-1057.

[19]Samson, R. J., Mulholland, G. W..], and Gentry, J. W., "Structural Analysis of Soot Agglomerates," *Langmuir*, Vol. 3, 1987, pp. 272-281.

[20]Wersborg, B.L., Howard, J.B., and Williams, G.C., "Physical Mechanisms in Carbon Formation in Flames," *Proceedings of the Combustion Institute*, Vol. 14, 1972, pp. 929-940.

[21]Urban, D.L., Yuan, Z.-G., Sunderland, P.B., Linteris, G.T., Voss, J.E., Lin, K.-C., Dai, Z., Sun, K., and Faeth, G.M., "Structure and Soot Properties of Nonbuoyant Ethylene/Air Laminar Jet Diffusion Flames," *AIAA Journal*, Vol. 36, No. 8, 1998, pp. 1346-1360.

[22]Urban, D.L., Yuan, Z.-G., Sunderland, P.B., Lin, K.-C., Dai, Z., and Faeth, G.M., "Smoke-Point Properties of Nonbuoyant Round Laminar Jet Diffusion Flames," *Proceedings of the Combustion Institute*, in press.

[23]Köylü, Ü.Ö., and Faeth, G.M., "Optical Properties of Overfire Soot in Buoyant Turbulent Diffusion Flames at Long Residence Times," *Journal of Heat Transfer*, Vol. 116, No. 1, 1994, pp. 152-159.

[24]Köylü, Ü.Ö., and Faeth, G.M., "Optical Properties of Soot in Buoyant Laminar Diffusion Flames," *Journal of Heat Transfer,* Vol. 116, No. 4, 1994, pp. 971-979.

[25]Farias, T.L., Carvalho, M.G., Köylü, Ü.Ö., and Faeth, G.M., "Computational Evaluation of Approximate Rayleigh-Debye-

Gans/Fractal-Aggregate Theory for the Absorption and Scattering Properties of Soot," *Journal of Heat Transfer*, Vol. 117, No. 1, 1995,pp. 152-159.

[26]Krishnan, S.S., Lin, K.-C., and Faeth, G.M., "Optical Properties in the Visible of Overfire Soot in Large Buoyant Turbulent Diffusion Flames," *Journal of Heat Transfer,* Vol. 122, No. 3, 2000, pp. 517-524.

[27]Neoh, K.G., Howard, J.B., and Sarofim, A.F., "Effect of Oxidation on the Physical Structure of Soot," *Proceedings of the Combustion Institute,* Vol. 20, 1984, pp. 951-957.

[28]Lahaye, J., and Prado, G., "Morphology and Internal Structure of Soot and Carbon Blacks," *Particulate Carbon*, (D.C. Siegla and G.W. Smith, eds.), Plenum Press, New York, 1981, pp. 33-55.

[29]Dobbins, R.A., Mulholland, G.W., and Bryner, N.P., "Comparison of a Fractal Smoke Optics Model with Light Extinction Measurements," *Atmospheric Environment,* Vol. 28, No. , 1994, pp. 889-897.

[30]Wu, J.-S., Krishnan, S.S., and Faeth, G.M., "Refractive Indices at Visible Wavelengths of Soot Emitted from Buoyant Turbulent Diffusion Flames," *Journal of Heat Transfer*, Vol. 119, No. 2, 1997, pp. 203-237.

[31]Dobbins, R.A., Fletcher, R.A., and Lu, W., "Laser Microprobe Analysis of Soot Precursor Particles and Carbonaceous Soot," *Combustion and Flame*, Vol. 100, Nos. 1 and 2, 1995, pp. 301-309.

[32]Dobbins, R.A., "The Early Soot Particle Formation in Hydrocarbon Flames," *Physical and Chemical Aspects of Combustion* (F.L. Dryer and R.F. Sawyer, eds.), Gordon and Breach, Amsterdam, 1997, pp. 107-133.

[33]Dobbins, R.A., Fletcher, R.A., and Chang, H.-C., "The Evolution of Soot Precursor Particles in a Diffusion Flame," *Combustion and Flame*, Vol. 115, No. 3, 1998, pp. 285-289.

[34]Vander Wal, R.L., "Soot Precursor Materials: Visualization Via Simultaneous LIF-LII and Characterization Via TEM," *Proceedings of the Combustion Institute*, Vol. 26, Nos. 1-6, 1996, pp. 2269-2275.

[35]Vander Wal, R.L., "A TEM Methodology for the Study of Soot Particle Structure," *Combustion Science and Technology*, Vol. 126, Nos. 1-6, 1997, pp. 333-357.

[36]Vander Wal, R.L., "Soot Precursor Carbonization: Visualization Using LIF-LII and Comparison Using Bright and Dark Field TEM," *Combustion and Flame*, Vol. 112, No. 4, 1998, pp. 607-616.

[37]Ishiguro, T., Takatori, Y., and Akihama, K., "Microstructure of Diesel Soot Particles Probed by Electron Microscopy: First Observations of Inner Core and Outer Shell," *Combustion and Flame*, Vol. 108, Nos. 1/2, 1997, pp. 231-234.

[38]Krishnan, S.S., Lin, K.-C., and Faeth, G.M., "Extinction and Scattering Properties of Soot Emitted from Large Buoyant Turbulent Diffusion Flames," *Journal of Heat Trans*fer, in press

[39]Megaridis, C.M., and Dobbins, R.A., "Morphological Description of Flame-Generated Materials," *Combustion Science and Technology*, Vol. 71, Nos. 1-3, 1990, pp. 95-109.

[40]Mountain, R.D., and Mulholland, G.W., "Light Scattering from Simulated Smoke Agglomerates," *Langmuir*, Vol. 4, 1988, pp. 1321-1326.

[41]Berry, M. V., and Percival, I. C., "Optics of Fractal Clusters Such as Smoke," *Optica Acta,* Vol. 33, 1986, pp. 577-591.

[42]Dobbins, R.A., and Megaridis, C.M., "Absorption and Scattering of Light by Polydisperse Aggregates," *Applied Optics*, Vol. 30, 1991, pp. 4747-4754.

[43]Sorensen, C.M., Cai, J., and Lu, N., "Test of Static Structure Factors for Describing Light Scattering from Fractal Soot Aggregates," *Langmuir,* Vol. 8, 1992, pp. 2064-2069.

[44]Puri, R., Richardson, T.F., Santoro, R.J., and Dobbins, R.A., "Aerosol Dynamic Processes of Soot Aggregates in a Laminar Ethene Diffusion Flame," *Combustion and Flame,* Vol. 92, No. 3, 1993, pp. 320-333.

[45]Magnussen, B.F., "An Investigation into the Behavior of Soot in a Turbulent Free Jet C_2-H_2-Flame," *Proceedings of the Combustion Inst*itute, Vol. 15, 1974, pp. 1415-1425.

[46]Kerker, M., *The Scattering of Light,* Academic Press, New York, 1969, pp. 414-486.

[47]van de Hulst, H.C., *Light Scattering by Small Particles*, Dover Publications, New York, 1957.

[48]Bohren, C.F., and Huffman, D.R., *Absorption and Scattering of Light by Small Particles*, Wiley, New York, 1983, pp. 477-482.

[49]Chen, H.Y., Iskander, M.F., and Penner, J.E., "Light Scattering and Absorption by Fractal Agglomerates and Coagulations of Smoke Aerosols," *Journal of Modern Optics,* Vol. 2, 1990, pp. 171-181.

[50]Ku, J.C., and Shim, K.-H., "Optical Diagnostics and Radiative Properties of Simulated Soot Agglomerates," *Journal of Heat Transfer,* Vol. 113, No. 4, 1992, pp. 953-958.

[51]Dalzell, W.H., and Sarofim, A.F., "Optical Constants of Soot and Their Application to Heat Flux Calculations," *Journal of Heat Transfer.* Vol. 91, No. 1, 1969, pp. 100-104.

[52]Stagg, B.J., and Charalampoulos, T.T., "Refractive Indices of Pyrolytic Graphite, Amorphous Carbon, and Flame Soot in the Temperature Range 25° to 600° C.," *Combustion and Flame*, Vol. 94, No. 4, 1993, pp. 381-396.

[53]Felske, J.D., Charalampopoulos, T.T., and Hura, H., "Determination of the Refractive Indices of Soot Particles from the Reflectivities of Compressed Soot Pellets," *Combustion Science and Technology*, Vol. 37, Nos. 5+6, 1984, pp. 263-284.

[54]Köylü, Ü.Ö., and Faeth, G.M., "Spectral Extinction Coefficients of Soot Aggregates from Turbulent Diffusion Flames," *Journal of Heat Transfer,* Vol. 118, No. 2, 1996, pp. 415-421.

[55]Tien, C. L., and Lee, S. C., "Flame Radiation," *Progress in Energy and Combustion Science*, Vol. 8, No. 1, 1982, pp. 41-59.

[56]Gore, J.P., and Faeth, G.M., "Structure and Spectral Radiation Properties of Turbulent Ethylene/Air Diffusion Flames," *Proceedings of the Combustion Institute*, Vol. 21, 1986, pp. 1521-1531.

[57]Gore, J.P., and Faeth, G.M., "Structure and Radiation Properties of Luminous Turbulent Acetylene/Air Diffusion Flames," *Journal of Heat Transfer,* Vol. 110, No. 1, 1988, pp. 173-181.

[58]Sunderland, P.B., Mortazavi, S., Faeth, G.M., and Urban, D.L., "Laminar Smoke Points of Nonbuoyant Jet Diffusion Flames," *Combustion and Flame,* Vol. 96, No. 1, 1994, pp. 97-103.

[59]Sunderland, P.B., Köylü, Ü.Ö., and Faeth, G.M., "Soot Formation in Weakly Buoyant Acetylene-Fueled Laminar Jet Diffusion Flames Burning in Air," *Combustion and Flame*, Vol. 100, Nos. 1/2, 1995, pp. 310-322.

[60]Sunderland, P.B., and Faeth, G.M., "Soot Formation in Hydrocarbon/Air Laminar Jet Diffusion Flames," *Combustion and Flame*, Vol. 105, Nos. 1/2, 1996, pp. 132-146.

[61]Lin, K.-C., and Faeth, G.M., "Hydrodynamic Suppression of Soot Emissions in Laminar Diffusion Flames," *Journal of Propulsion and Power*, Vol. 12, No. 1, 1996, pp. 10-17.

[62]Santoro, R.J., Semerjian, H.B., and Dobbins, R.A., "Soot Particle Measurements in Diffusion Flames," *Combustion and Flame*, Vol. 51, No. 2, 1983, pp. 203-218.

[63]Santoro, R.J., Yeh, T.T., Horvath, J.J., and Semerjian, H.G., "The Transport and Growth of Soot Particles in Laminar Diffusion Flames," *Combustion Science and Technology*, Vol. 53, Nos. 2+3, 1987, pp. 89-115.

[64]Puri, R., Richardson, T.F., Santoro, R.J., and Dobbins, R.A., "Aerosol Dynamic Processes of Soot Aggregates in a Laminar Ethene Diffusion Flame," *Combustion and Flame,* Vol. 92, No. 3, 1993, pp. 320-333.

[65]Puri, R., Santoro, R.J., and Smyth, K.C., "The Oxidation of Soot and Carbon Monoxide in Hydrocarbon Diffusion Flames," *Combustion and Flame*, Vol. 97, No. 2, 1994, pp. 125-144.

[66]Spalding, D. B., *Combustion and Mass Transfer*, Pergamon Press, New York, 1979, pp. 185-195.

[67]Kuo, K.K., *Principles of Combustion*, Wiley, New York, 1986, pp. 360-370.

[68]Xu, F., and Faeth, G.M., "Soot Formation in Laminar Acetylene/Air Diffusion Flames at Atmospheric Pressure," *Combustion and Flame*, in press.

[69]Xu, F., El-Leathy, A.M., and Faeth, G.M., "Soot Oxidation in Hydrocarbon/Air Diffusion Flames at Atmospheric Pressure," *Combustion and Flame*, submitted.

[70]Kang, K.T., Hwang, J.Y., Chung, S.M., and Lu, W., "Soot Zone Structure and Sooting Limit in Diffusion Flames: Comparison of Counterflow and the Co-flow

Flames," *Combustion and Flame,* Vol. 109, Nos. 1/2, 1997, pp. 266-281.

[71]Lin, K.-C., and Faeth, G.M., "Shapes of Nonbuoyant Round Luminous Hydrocarbon/Air Laminar Jet Diffusion Flames." *Combustion and Flame,* Vol. 116, No. 3, 1998, pp. 415-431

[72]Sunderland, P.B., Mendelson, B.J., Yuan, Z.-G., and Urban, D.L., "Shapes of Buoyant and Nonbuoyant Laminar Jet Diffusion Flames," *Combustion and Flame,* Vol. 116, No. 3, 1999, pp. 376-386.

[73]Urban, D.L., Yuan, Z.-G., Sunderland, P.B., Lin, K.-C., Dai, Z., and Faeth, G.M.. "Smoke-Point Properties of Nonbuoyant Round Laminar Jet Diffusion Flames," *Proceedings of the Combustion Institute,* in press.

[74]Dai, Z., and Faeth, G.M., "Hydrodynamic Suppression of Soot Formation in Laminar Coflowing Jet Diffusion Flames," *Proceedings of the Combustion Institute,* in press.

[75]Law, C.K., and Faeth, G.M., "Opportunities and Challenges of Combustion in Microgravity," *Progress in Energy and Combustion Science*, Vol. 20, No. 1, 1994, pp. 65-113.

[76]Bockhorn, H., Fetting, F., Wannemacher, G., and Wentz, H. W., "Optical Studies of Soot Particle Growth in Hydrocarbon Oxygen Flames," *Proceedings of the Combustion Institute*, Vol. 19, 1982, pp. 1413-1420.

[77]Bockhorn, H., Fetting, F., Heddrich, A., and Wannemacher, G., "Investigation of the Surface Growth of Soot in Flat Low Pressure Hydrocarbon Oxygen Flames," *Proceedings of the Combusion Institute*, Vol. 20, 1984, pp. 979-988.

[78]Wieschnowsky, U., Bockhorn, H., and Fetting, F., "Some New Observations Concerning the Mass Growth of Soot in Premixed Hydrocarbon/Oxygen Flames," *Proceedings of the Combustion Institute*, Vol. 22, 1988, pp. 343-352.

[79]Mauss, F., Schäfer, T., and Bockhorn, H., "Inception and Growth of Soot Particles and Dependence on Surrounding Gas Phase," *Combustion and Flame*, Vol. 99, Nos. 3/4, 1994, pp. 687-705.

[80]Mauss, F., Trilken, B., Breitbach, H., and Peters, N., "Soot Formation in Partially Premixed Diffusion Flames at Atmospheric Pressure," *Soot Formation in Combustion* (H. Bockhorn, ed.), Springer-Verlag, Berlin, 1994, pp. 325-349.

[81]Balthasar, M., Heyl, A., Mauss, F., Schmitt, F., and Bockhorn, H., "Flamelet Modeling of Soot Formation in Laminar EthyleneAir-Diffusion Flames," *Proceedings of the Combustion Institute,* Vol. 26, 1996, pp. 2369-2377.

[82]Bai, K.W., Balthasar, M., Mauss, F., and Fuchs, L., "Detailed Soot Modeling in Turbulent Jet Diffusion Flames," *Proceedings of the Combustion Institute,* Vol. 27, 1998, pp. 1623-1630.

[83]Harris, S.J., and Weiner, A.M., "Surface Growth of Soot Particles in Premixed Ethylene/Air Flames," *Combustion Science and Technology*, Vol. 31, Nos. 3 and 4, 1983, pp. 155-167.

[84]Harris, S.J., and Weiner, A.M., "Determination of the Rate Constant for Soot Surface Growth," *Combustion Science and Technology*, Vol. 32, Nos. 5 and 6, 1983, pp. 267-275.

[85]Harris, S.J., and Weiner, A.M., "Soot Particle Growth in Premixed Toluene/Ethylene Flames," *Combustion Science and Technology*, Vol. 38, Nos. 1 and 2, 1984, pp. 75-87.

[86]Harris, S.J., and Weiner, A.M., "Some Constraints on Soot Particle Inception In Premixed Ethylene Flames," *Proceedings of the Combustion Inst*itute, Vol. 20, 1984, pp. 969-978.

[87]Harris, S.J., and Weiner, A.M., "A Picture of Soot Particle Inception," *Proceedings of the Combustion Inst*itute, Vol. 22, 1988, pp. 333-342.

[88]Harris, S.J., "Soot Particle Inception and O_2 Profiles in a Premixed Ethylene Flame," *Combustion and Flame*, Vol. 66, No. 2, 1986, pp. 211-214.

[89]Harris, S.J., Weiner, A.M., Blint, R.J., and Goldsmith, J.E.M., "Concentration Profiles in Rich and Sooting Ethylene Flames," *Proceedings of the Combustion Inst*itute, Vol. 21, 1986, pp. 1033-1045.

[90]Ramer, E.R., Merklin, J.F., Sorensen, C.M., and Taylor, T.W. "Chemical and Optical Probing of Premixed Methane/Oxygen Flames," *Combustion Science and Technology*, Vol. 48, Nos. 5 and 6, 1986, pp. 241-255.

[91]Matzing, H., and Wagner, H.Gg., "Measurements About the Influence of Pressure on Carbon Formation in Premixed Laminar C_2H_2-Air Flames," *Proceedings of the Combustion Institute*, Vol. 21, 1996, pp. 1047-1055.

[92]Böhm, H., Hesse, D., Jander, H., Lüers, B., Pietscher, J., Wagner, H.Gg., and Weiss, M., "The Influence of Pressure and Temperature on Soot Formation in Premixed Flames," *Proceedings of the Combustion Institute*, Vol. 22, 1988, pp. 403-411.

[93]Böhm, H., Felderman, Chr., Heidermann, Th., Jander, H., Lüers, B., and Wagner, H.Gg., "Soot Formation in Premixed C_2H_2-Air Flames for Pressures Up to 100 Bar," *Proceedings of the Combustion Institute*, Vol. 24, 1992, pp. 991-997.

[94]Böhnig, M., Feldermann, Chr. Jander, H., Lüers, B., Rudolph, G., and Wagner, H.Gg., "Soot Formation in Premixed C_2H_2 Flat Flames at Elevated Pressures," *Proceedings of the Combustion Institute*, Vol. 23, 1990, pp. 1581-1587

[95]Hanesch, S., Jander, H., Pope, Th., and Wagner, H. Gg., "Soot Mass Growth and Coagulation of Soot Particles in C_2/H_2/Air-Flames at 15 Bar," *Proceedings of the Combustion Institute*, Vol. 25, 1994, pp. 577-584.

[96]Lam, F.W., Howard, J.B., and Longwell, J.P. "The Behavior of Polycyclic Aromatic Hydrocarbons During the Early Stages of Soot Formation," *Proceedings of the Combustion Institute*, Vol. 22, 1988, pp. 323-332.

[97]Lam, F.W., Longwell, J.P., and Howard, J.B., "The Effect of Ethylene and Benzene Addition of the Formation of Polycyclic Aromatic Hydrocarbons, and Soot in a Jet-Stirred/Plug-Flow Combustor," *Proceedings of the Combustion Institute*, Vol. 23, 1990, p. 1477-1484.

[98]McKinnon, J.T., and Howard, J.B., "The Roles of PAH and Acetylene in Soot Nucleation and Growth," *Proceedings of the Combustion Institute*, Vol. 24, 1992, p. 965-971.

[99]Lafleur, A.L., Howard, J. B., Taghizadeh, K., Plummer, E.B., Scott, L.T., Necula, A. and Swallow, K.C., "Identification of $C_{20}H_{10}$ Dicyclopentapyrenes in Flames: Correlation with Corannulinee and Fullerene Formation," *Journal of Physical Chemistry*, 1996, pp. 17421-17428.

[100]Benish, T.G., Lafleur, A.L., Taghizadeh, K., and Howard, J.B., "C_2H_2 and PAH as Soot Growth Reactants in Premixed C_2H_4-Air Flames," *Proceedings of the Combustion Institute*, Vol. 26, 1996, pp. 2319-2326.

[101]Richter, H. and Howard, J.B., "Formation of Polycyclic Aromatic Hydrocarbons and Their Growth to Soot — A Review of Chemical Reaction Pathways," *Progress in Energy and Combustion Science*, Vol. 26, Nos. 4-6, 2000, pp. 565-608.

[102]Macadam, S., Hoffman, A.B., Beér, J.M., and Sarofim, A.F., "Soot Surface Growth by Polycyclic Aromatic Hydrocarbon and Acetylene Addition," *Proceedings of the Combustion Institute*, Vol. 26, 1996, pp. 2295-2302.

[103]Smedley, J.M., Williams, A., and Bartle, K.D., "A Mechanism for the Formation of Soot Particles and Soot Deposits," *Combustion and Flame*, Vol. 91, No. 1, 1992, p. 71-82.

[104]D'Alessio, A., D'Anna, A., D'Orsi, A., Minutolo, P., Barbella, R., and Ciajolo, A., "Precursor Formation on Soot Inception in Premixed Ethylene Flames", *Proceedings of the Combustion Institute*, Vol. 24, 1992, pp. 973-980.

[105]D'Anna, A., D'Alessio, A., and Minutolo, P., "Spectroscopic and Chemical Characterization of Soot Inception Process in Premixed Laminar Flames at Atmospheric Pressure," *Soot Formation in Combustion* (H. Bockhorn, ed.), Springer-Verlag, Berlin, 1994, pp. 83-103.

[106]Frenklach, M., and Wang, H. "Detailed Modeling of Soot Particle Nucleation and Growth," *Proceedings of the Combustion Institute*, Vol. 23, 1990, pp. 1559-1556.

[107]Frenklach, M., and Wang, H., "Detailed Mechanism and Modeling of Soot Particle Formation," *Soot Formation in Combustion* (H. Bockhorn, ed.), Springer-Verlag, Berlin, 1994, p. 165-192.

[108]Kazakov, A., Wang, H., and Frenklach, M., "Detailed Modeling of Soot Formation in Laminar Premixed Ethylene Flames at a Pressure of 10 Bar," *Combustion and Flame*, Vol. 100, Nos. 1/2, 1995, pp. 111-120.

[109]Frenklach, M., "On the Surface Growth Mechanism of Soot Particles," *Proceedings of the Combustion Institute*, Vol. 26, 1996, pp. 2285-2293.

[110]Kazakov, A., and Frenklach, M., "On the Relative Contribution of Acetylene and Aromatics to Soot Particle Surface Growth," *Combustion and Flame,* Vol. 112, Nos. 1/2, 1998, pp. 270-274.

[111]Colket, M.B., and Hall, R.J., "Successes and Uncertainties in Modeling Soot Formation in Laminar Premixed Flames," *Soot Formation in Combustion* (H. Bockhorn, ed.), Springer-Verlag, Berlin, 1994, p. 442-470.

[112]Xu, F., Sunderland, P.B., and Faeth, G.M., "Soot Formation in Laminar Premixed Ethylene/Air Flames at Atmospheric Pressure," *Combustion and Flame*, Vol. 108, No. 4, 1997, pp. 471-493.

[113]Xu, F., Lin, K.-C., and Faeth, G.M., "Soot Formation in Laminar Premixed Methane/Oxygen Flames at Atmospheric Pressure," *Combustion and Flame*, Vol. 115, Nos. 1/2, 1998, pp. 195-209.

[114]Xu, F., and Faeth, G.M., "Structure of the Soot Growth Region of Laminar Premixed Methane/Oxygen Flames," *Combustion and Flame*, Vol. 121, No. 4, 2000, pp. 640-650.

[115]Leung, K.M., Lindstedt, R.P., and Jones, W.P., "A Simplified Reaction Mechanism for Soot Formation in Nonpremixed Flames," *Combustion and Flame,* Vol. 87, Nos. 3 and 4, 1991, pp. 289-305.

[116]Leung, K.M., and Lindstedt, R.P., "Detailed Kinetic Modeling of C_1-C_3 Alkane Diffusion Flames," *Combustion and Flame,* Vol. 102, Nos. 1 and 2, 1995, pp. 129-160.

[117]Kee, R.J., Grcar, J.F., Smooke, M.D., and Miller, J.A., "A FORTRAN Program for Modeling Steady Laminar One-Dimensional Premixed Flames," Report No. SAND85-8240, Sandia National Laboratories, Albuquerque, 1985.

[118]Chase, M.W., Jr., Davies, C.A., Downey, J.R., Jr., Frurip, D.J., McDonald, R.A., and Syverud, A.N., *JANAF Thermochemical Tables*, 3rd ed., *Journal of Physical Chemistry Reference Data*, Vol. 14, Supplement No. 1, 1986, p. 1211.

[119]Lin, K.-C., and Faeth, G.M., "Effects of Hydrodynamics on Soot Formation in Hydrocarbon-Fueled Laminar Opposed Jet Flames," *Journal of Propulsion and Power*, Vol. 12, No. 4, 1996, pp. 691-698.

[120]Lin, K.-C., and Faeth, G.M. "Structure of Laminar Permanently-Blue Opposed-Jet Ethylene-Fueled Diffusion Flames," *Combustion and Flame,* Vol. 115, No. 4, 1998, pp. 468-480.

[121]Puri, R., Moser, H., Santoro, R.J., and Smyth, K.C., "Laser-Induced Fluorescence Measurements of OH Concentrations in the Oxidation Region of Laminar, Hydrocarbon Diffusion Flames," *Proceedings of the Combustion Institute*, Vol. 24, pp. 1015-1022.

[122]Garo, A., Lahaye, J., and Prado, G., "Mechanisms of Formation and Destruction of Soot Particles in a Laminar Methane-Air Diffusion Flame," *Proceedings of the Combustion Institute,* Vol. 21, 1986, pp. 1023-1031.

[123]Garo, A., Prado, G., and Lahaye, J., "Chemical Aspects of Soot Particles Oxidation in a Laminar Methane-Air Diffusion Flame," *Combustion and Flame*, Vol. 79, Nos. 3 and 4, 1990, pp. 226-233.

[124]Haudiquert, M., Cessou, A., Stepowski, D., and Coppalle, A., "OH and Soot Concentration Measurements in a High-Temperature Laminar Diffusion Flame," *Combustion and Flame,* Vol. 111, No. 4, 1997, pp. pp. 338-349.

[125]Mitchell, R.E., Sarofim, A.F., and Clomberg, L.A., "Experimental and Numerical Investigation of Confined Laminar Diffusion Flames," *Combustion and Flame*, Vol. 37, No. 3, 1980, pp. 227-244.

[126]Smooke, M.D., Mitchell, R.E., and Keyes, D.E., "Numerical Solution of Two-Dimensional Axisymmetric Laminar Diffusion Flames," *Combustion Science and Technology*, Vol. 67, Nos. 1-3, 1989, pp. 85-122.

[127]Smooke, M.D., Lin, J.K., and Long, M.B., "Computational and Experimental Study of a Laminar Axisymmetric Methane-Air Diffusion Flame," *Proceedings of the Combustion Institute*, Vol. 23, 1990, pp. 575-582.

[128]Smooke, M.D., Xu, Y., Zurn, R.M., Lin, P., Frank, J.H. and Long, M.B., "Computational and Experimental Study of OH and CH Radicals in Axisymmetric Laminar Diffusion Flames," *Proceedings of*

the Combustion Institute, Vol. 24, 1992, pp. 813-821.

[129]Norton, T.S., Smyth, K.C., Miller, J.H., and Smooke, M.D., "Comparison of Experimental and Computed Species Concentration and Temperature Profiles in Laminar, Two-Dimensional Methane/Air Diffusion Flames," *Combustion Science and Technology*, Vol. 90, Nos. 1-4, 1993, pp. 1-34.

[130]Smooke, M.D., Ern, A., Tanoff, M.A., Valdati, B.A., Mohammed, R.K., Marran, D.F. and Long, M.B., "Computational and Experimental Study of NO in an Axisymmetric Laminar Diffusion Flame," *Proceedings of the Combustion Institute*, Vol. 26, pp. 2161-2170.

[131]Walsh, K.T., Long, M.B., Tanoff, M.A. and Smooke, M.D., "Experimental and Computational Study of CH, CH*, and OH* in an Axisymmetric Laminar Diffusion Flame," *Proceedings of the Combustion Institute*, Vol. 27, 1998, pp. 615-623.

[132]Smooke, M.D., McEnally, C.S., Pfefferle, L.D., Hall, D.J., and Colket, M.B., "Computational and Experimental Study of Soot Formation on a Coflow, Laminar Diffusion Flame," *Combustion and Flame,* Vol. 117, Nos. 1/2, 1999, pp. 117-139.

[133]Walsh, K.T., Fielding, J., Smooke, M.D. and Long, M.B., "Experimental and Computational Study of Temperature, Species and Soot in Buoyant and Nonbuoyant Coflow Laminar Diffusion Flames, *Proceedings of the Combustion Institute*, in press.

[134]Saito, K., Williams, F.A., and Gordon, A.S., "Structure of Laminar Coflow Methane-Air Diffusion Flames," *Journal of Heat Transfer,* Vol. 108, No. 3, 1986, pp. 640-648.

[135]McEnally, C.S., and Pfefferle, L.D., "Aromatic and Linear Hydrocarbon Concentration Measurements in a Non-Premixed Flame," *Combustion Science and Technology,* Vols. 115-117, Nos. 1-6, 1996, pp. 183-209.

[136]McEnally, C.S., and Pfefferle, L.D., "Flow Time Effects on Hydrocarbon Growth and Soot Formation in Coflowing Methane/Air Non-Premixed Flames," *Proceedings of the Combustion Institute,* Vol. 27, 1998, pp. 1539-1547.

[137]McEnally, C.S., Schaffer, A.M., Long, M.B., Pfefferle, L.D., Smooke, M.D., Colket, M.B., and Hall, R.J., "Computational and Experimental Study of Soot Formation in a Coflow Laminar Ethylene Diffusion Flame," *Proceedings of the Combustion Institute*, Vol. 27, 1998, pp. 1497-1505.

[138]McEnally, C.S., Pfefferle, L.D., Schaffer, A.M., Long, M.B., Smooke, M.D., and Colket, M.B., "Characterization of Coflowing Methane/Air Non-Premixed Flame with Computer Modeling, Rayleigh-Raman Imaging and On-Line Mass Spectrometry," *Proceedings of the Combustion Institute*, in press.

[139]El-Leathy, A.M., Xu, F., and Faeth, G.M., "Soot Growth in Hydrocarbon-Fueled Laminar Diffusion Flames at Atmospheric Pressure," AIAA Paper No. 2001-1077, 2001.

[140]Nagle, J., and Strickland-Constable, R.F., "Oxidation of Carbon Between 1000-2000 °C," *Proceedings of Fifth Carbon Conference*, Vol. 1, 1962, pp. 154-164.

[141]Neoh, K.G., Howard, J.B., and Sarofim, A.F., "Soot Oxidation in Flames," *Particulate Carbon* (D.C. Siegla and B.W. Smith, ed.), Plenum Press, New York, 1980, pp. 261-277.

[142]Tesner, P.A., "Formation of Dispersed Carbon by Thermal Decomposition of Hydrocarbons," *Proceedings of the Combustion Institute,* Vol. 7, 1958, pp. 546-556.

[143]Tesner, P.A., "Dispersed Carbon Formation by Acetylene Self-Combustion," *Proceedings of the Combustion Institute,* Vol. 8, 1960, pp. 627-633.

[144]Radcliffe, S.W., and Appleton, J.P., "Soot Oxidation Rates in Gas Turbine Engines," *Combustion Science and Technology*, Vol. 4, No. 2, 1971, pp. 171-175.

[145]Park, C., and Appleton, J.P., "Shock-Tube Measurements of Soot Oxidation Rates," *Combustion and Flame,* Vol. 20, No. 3, 1973, pp. 369-379.

[146]Rosner, D.E., and Allendorf, H.D., "Comparative Studies of the Attack of Pyrolytic and Isotropic Graphite by Atomic and Molecular Oxygen at High Temperatures," *AIAA Journal* , Vol. 6, No. 5, 1968, pp. 650-

[147]Wright, F.J., "The Oxidation of Soot by O Atoms," *Proceedings of the Combustion Institute*, Vol. 15, 1974, pp. 1449-1460.

[148]Fenimore, C.P., and Jones, G.W., "Oxidation of Soot by Hydroxyl Radicals," *J. Phys. Chem.*, Vol. 71, 1967, pp. 593-597.

[149]Mulcahy, M.F.R., and Young, B.C., *Carbon*, Vol. 13, 1975, p. 115.

[150]Wicke, B.C., Wong, C., and Grady, K.A., "Room Temperature Oxidation of Soot by Oxygen Atoms," *Combustion and Flame,* Vol. 66, No. 1, 1986, pp. 37-46.

[151]Wicke, B.C., and Grady, K.A., "Nitric Oxide Inhibition by Soot Oxidation by Oxygen Atoms at 298 K," *Combustion and Flame,* Vol. 69, No. 2, 1987, pp. 185-192.

[152]Roth, P., Brandt, O., and von Gersum, S., "High Temperature Oxidation of Suspended Soot Particles Verified by CO and CO_2 Measurements," *Proceedings of the Combustion Institute*, Vol. 23, 1990, pp. 1485-1491.

[153]Libby, P.A., and Blake, T.R., "Theoretical Study of Burning of Carbon Particles," *Combustion and Flame*, Vol. 36, No. 2, 1979, pp. 139-169.

[154]Libby, P.A., and Blake, T.R., "Burning of Carbon Particles in the Presence of Water Vapor," *Combustion and Flame,* Vol. 41, No. 2, 1981, pp. 123-147.

[155]Johnstone, J.F., Chen, C.Y., and Scott, D.S., "Kinetics of the Steam-Carbon Reaction in Porous Graphite," *Industrial Engineering Chemistry,* Vol. 44, 1952, pp. 1564-1569.

[156]Bradley, D., Dixon-Lewis, G., El-Din Habik, S., and Mushi, E.M.J., "The Oxidation of Graphite Powder in Flame Reaction Zones," *Proceedings of the Combustion Institute,* Vol. 20, 1984, pp. 931-940.

[157]Puri, R., Santoro, R.J., and Smyth, K.C., "The Oxidation of Soot and Carbon Monoxide in Hydrocarbon Diffusion Flames," *Combustion and Flame*, Vol. 102, Nos. 1/2, 1995, pp. 226-228.

[158]Stein, S.E., and Fahr, A., "High-Temperature Stabilities of Hydrocarbons," *Journal of Physical Chemistry,* Vol. 89, 1985, pp. 3714-3725.

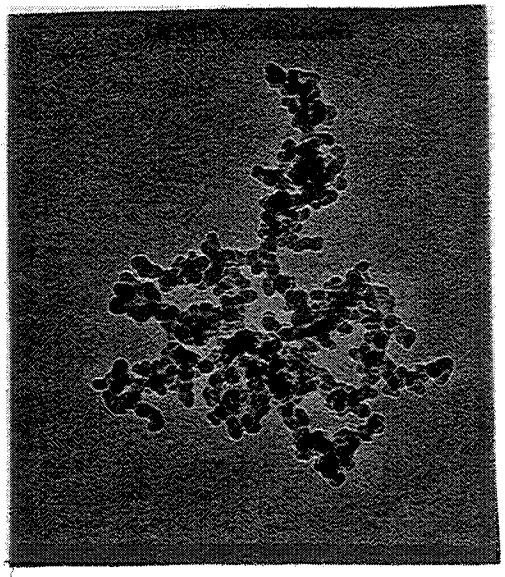

Fig. 1 TEM photograph of a soot particle emitted from a nonbuoyant round ethylene-fueled diffusion flame in still air at 100 kPa. Maximum dimension of the particle is roughly 1100 nm. From Urban et al.

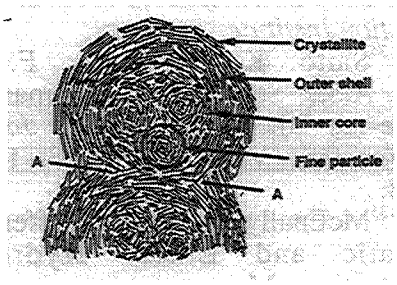

Fig. 2 Sketch of the structure of soot emitted from a diesel engine. From Ishiguro et al.[37]

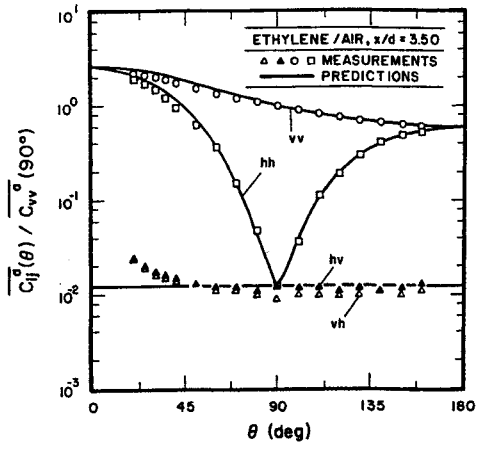

Fig. 3 Measured and predicted (RDG-PFA theory) scattering patterns for small soot aggregates in the fuel-rich region of a laminar ethylene-air diffusion flame. From Köylü and Faeth.[24]

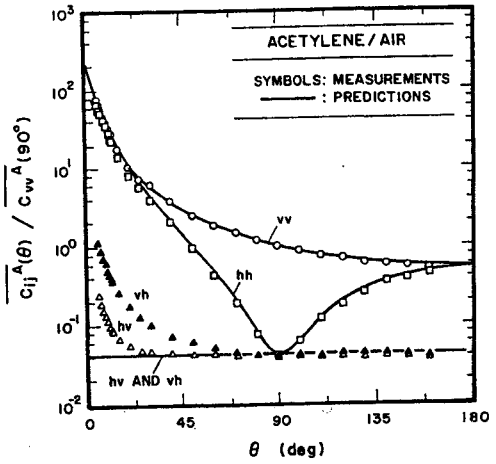

Fig. 4 Measured and predicted (RDG-PFA theory) scattering patterns for large soot aggregates emitted from an acetylene/air buoyant turbulent diffusion flame in the long residence time regime. From Wu et al.[30]

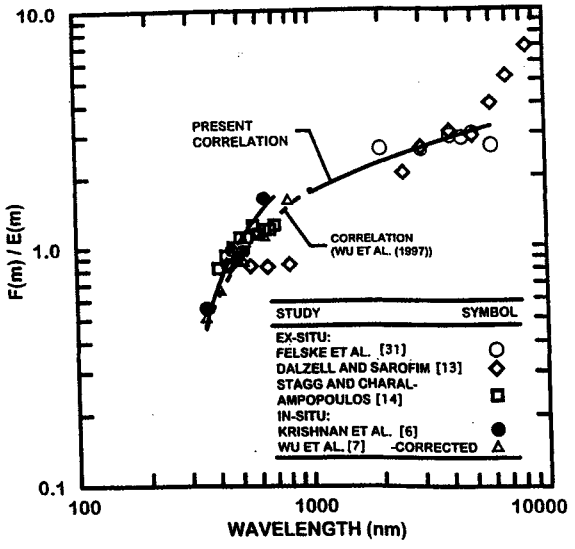

Fig. 5 Measurements of the refractive index ratio, F(m)/E(m) for various fuels as a function of wavelength for wavelengths of 250-10000 nm. Measurements of Dalzell and Sarofim,[51] Stagg and Charalampopoulos,[52] Krishnan et al.,[26] and Wu et al.[30] From Krishnan et al.[38]

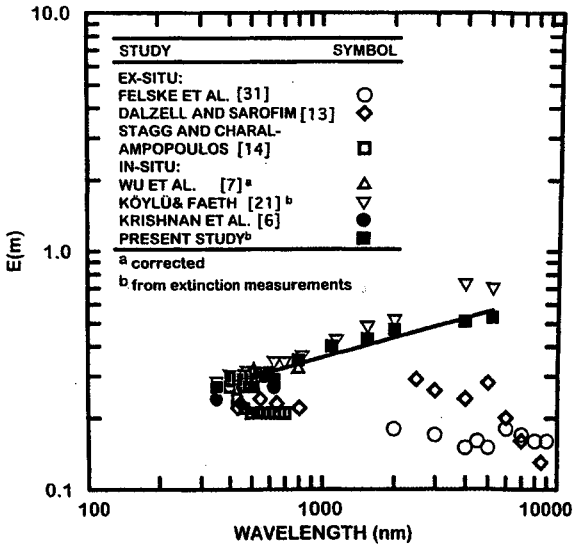

Fig. 6 Measurements of the refractive index function for absorption, E(m), as a function of wavelength for wavelengths of 250-10000 nm. Measurements of Dalzell and Sarofim,[51] Stagg and Charalampopoulos,[52] Felske et al.,[53] Krishnan et al.,[26] Wu et al.[30] and Köylü and Faeth.[54]

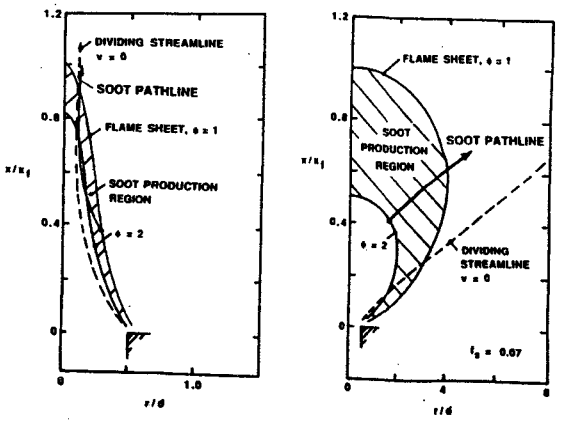

Fig. 7 Sketches of soot formation and oxidation regions and soot paths in buoyant and nonbuoyant hydrocarbon-fueled laminar jet diffusion flames in still air. From Urban et al.[21]

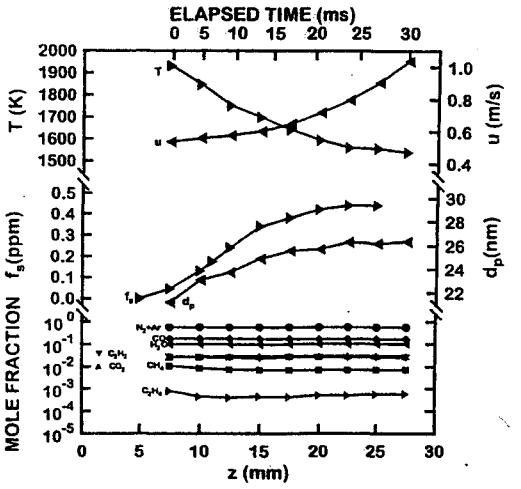

Fig. 8 Soot and flame properties along the axis of a laminar premixed ethylene/air flame burning at a C/O ratio of 0.88 at atmospheric pressure. From Xu et al.[112]

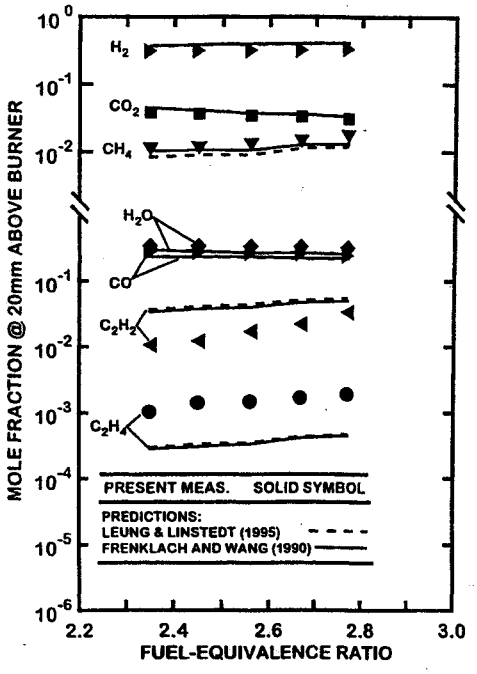

Fig. 9 Measured and predicted concentrations of major gas species at the axis of laminar premixed ethylene/air flames having various fuel-equivalence ratios at atmospheric pressure for z = 20 mm. From Xu et al.[112]

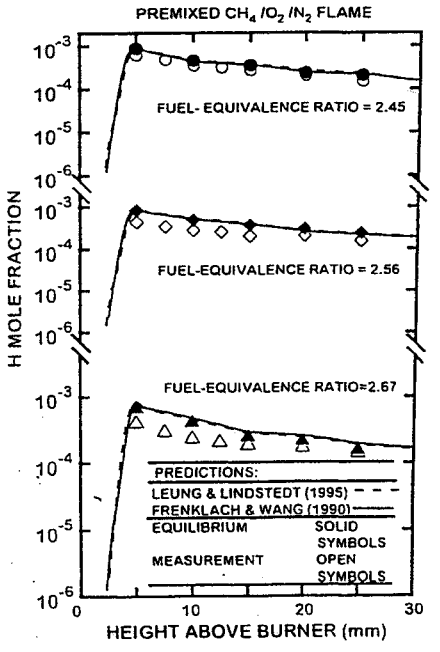

Fig. 10 Measured and predicted H-atom concentrations along the axes of laminar premixed methane/oxygen/nitrogen flames having various fuel-equivalence ratios at atmospheric pressure. From Xu et al.[114]

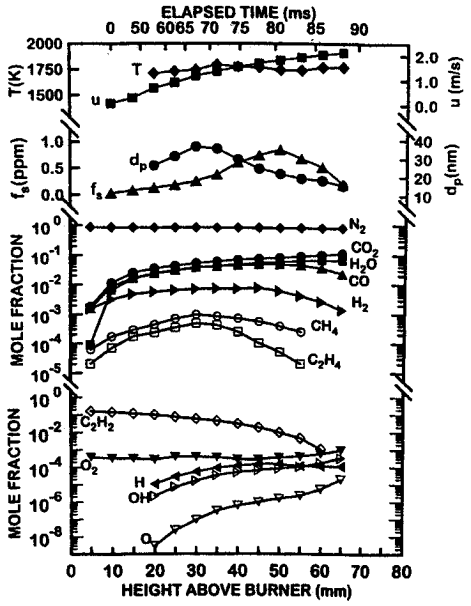

Fig. 11 Measured soot and flame properties along the axis of an acetylene (15.1% by volume)-nitrogen (84.9% by volume)/air diffusion flame at atmospheric pressure. From Xu et al.[68]

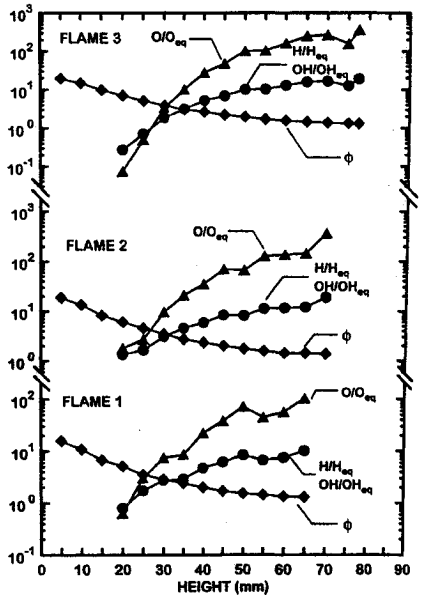

Fig. 12 Measured superequilibrium ratios along the axes of acetylene-nitrogen/air diffusion flames at atmospheric pressure. From Xu et al.[69]

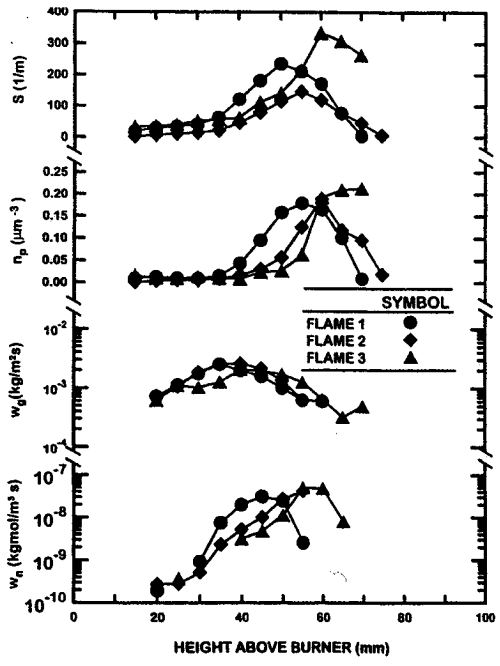

Fig. 13 Derived soot formation properties (S, n_p, w_n, w_g) along the axes of acetylene-nitrogen/air laminar jet diffusion flames at roughly atmospheric pressure. From Xu et al.[68]

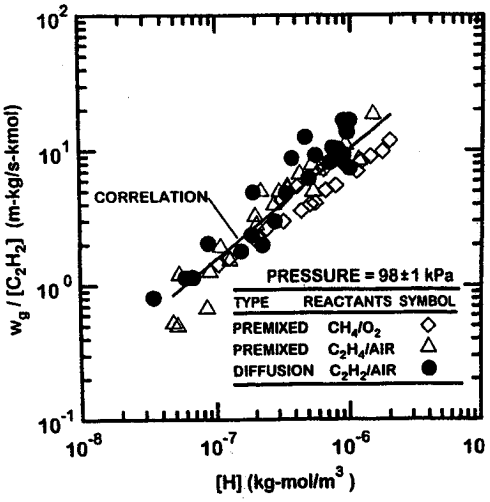

Fig. 14 Soot surface growth rates (corrected for soot oxidation) as a function of acetylene and hydrogen-atom concentrations for laminar premixed and diffusion flames at roughly atmospheric pressure. Measurements of ethylene/air premixed flames from Xu et al.,[112] measurements of methane/oxygen premixed flames from Xu et al.[113] and measurements of acetylene-nitrogen/air diffusion flames from Xu et al.[68]

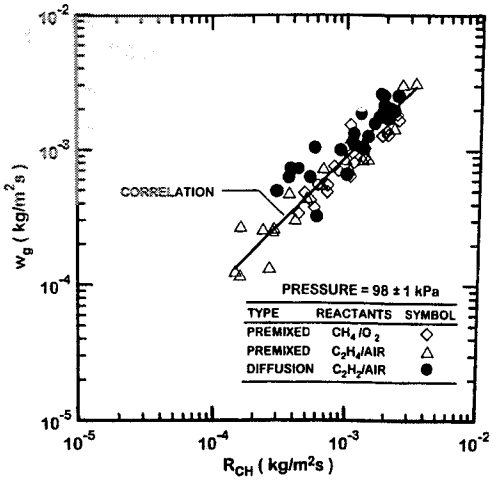

Fig. 15 Soot surface growth rates (corrected for soot oxidation) in terms of the HACA mechanism of Colket and Hall for premixed and diffusion flames at roughly atmospheric pressure. Measurements of ethylene/air premixed flames from Xu et al.,[112] measurements of methane/oxygen premixed flames from Xu et al.[113] and measurements of acetylene-nitrogen/air diffusion flames from Xu et al.[68]

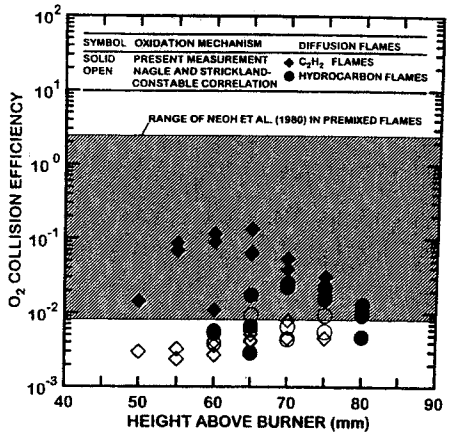

Fig. 16 Collision efficiencies assuming soot burnout due to attack by O_2 as a function of height above the burner. Found from the measurements of Neoh et al.[141] in premixed flames, estimated from the predictions of Nagle and Strickland-Constable[140] for the conditions of the diffusion flames, and found from direct measurements in the test diffusion flames from Xu et al.[69]

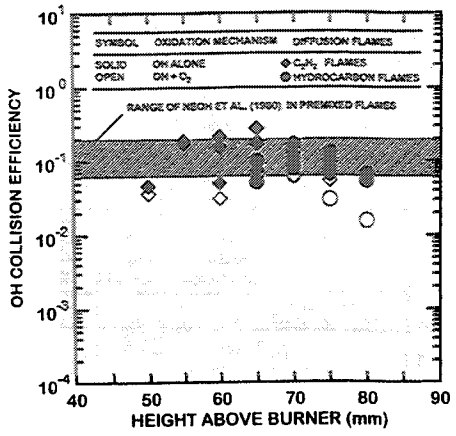

Fig. 17 Collision efficiencies assuming soot burnout due to attack by OH as a function of height above the burner. Found from the measurements of Neoh et al.[141] in premixed flames, and found from direct measurements in the test diffusion flames with and without parallel O_2 attack estimated from the predictions of Nagle and Strickland-Constable.[140]

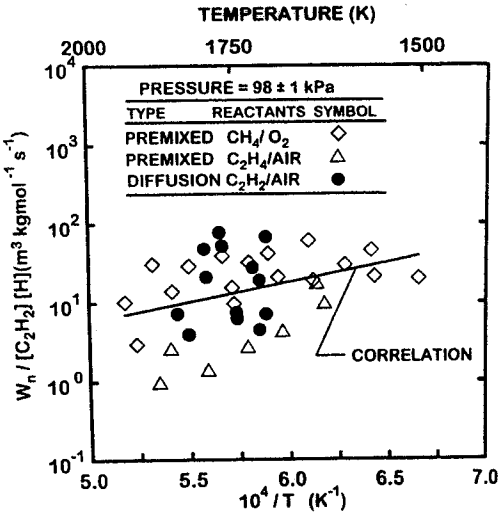

Fig. 18 Soot primary particle nucleation rates as a function of acetylene and H concentrations for laminar premixed and diffusion flames at atmospheric pressure. Measurements in ethylene/air premixed flames from Xu et al.,[112] measurements of methane/oxygen premixed flames from Xu et al.,[113] and measurements of acetylene-nitrogen/air diffusion flames from Xu et al.[114]